PROCEEDINGS A

royalsocietypublishing.org/journal/rspa

Research

Cite this article: Breunung T, Kogelbauer F, Haller G. 2022 The deterministic core of stochastically perturbed nonlinear mechanical systems. *Proc. R. Soc. A* **478**: 20210933. https://doi.org/10.1098/rspa.2021.0933

Received: 10 December 2021
Accepted: 17 May 2022

Subject Areas:
mechanical engineering, applied mathematics

Keywords:
nonlinear normal modes, reduced order modelling, stochastic dynamical systems, spectral submanifolds, Gaussian white noise, diffusion barriers

Author for correspondence:
Thomas Breunung
e-mail: thomasbr@umd.edu

†Present address: Department of Mechanical Engineering, University of Maryland, College Park, MD 20742, USA.

THE ROYAL SOCIETY PUBLISHING

The deterministic core of stochastically perturbed nonlinear mechanical systems

Thomas Breunung[1], Florian Kogelbauer[2] and George Haller[1]

[1]Institute for Mechanical Systems, ETH Zürich, Leonardstrasse 21 8092 Zürich, Switzerland
[2]Mathematics for Advanced Materials-OIL, AIST-Tohoku University, Sendai 980-8577, Japan

TB, 0000-0001-7885-2201; GH, 0000-0003-1260-877X

Invariant manifolds, such as normally hyperbolic invariant manifolds and spectral submanifolds, are the key to understanding the dynamical behaviour of many nonlinear mechanical systems and serve as natural candidates for model-order reduction. While numerous related invariant manifold results are available for unforced and periodically forced nonlinear mechanical systems, their applicability to random external forcing remains to be established. Here, we clarify the continued role of deterministic invariant manifolds, more specifically normally hyperbolic invariant manifolds and spectral submanifolds under the addition of small white noise excitation. Subsequently, we demonstrate our results on several mechanical systems.

1. Introduction

Modern analysis of deterministic dynamical systems relies on the understanding of influential invariant manifolds, such as centre manifolds, (un-) stable manifolds (e.g. Guckenheimer & Holmes [1]) or normally hyperbolic invariant manifolds (NHIMs) (e.g. Wiggins [2]). For realistic engineering structures, however, one has to account for parameter uncertainty, unmodelled degrees-of-freedom or unknown disturbances (e.g. Lutes & Sarkani [3]). Whether the aforementioned deterministic manifolds are of relevance under uncertainties or random external excitation has remained unclear.

Specifically for deterministic nonlinear mechanical systems, various invariant manifolds have been identified as relevant. For example, nonlinear normal modes have been defined either as manifolds of conservative periodic orbits (Kerschen *et al.* [4] for a review) or as invariant manifolds tangent to spectral subspaces of the linearized dynamics (Shaw & Pierre [5]). More recently, Haller & Ponsioen [6] identified the smoothest nonlinear continuation of a spectral subspace of the linearized dynamics as a spectral submanifold (SSM). While SSMs have recently been shown to provide exact reduced order models (e.g. Jain *et al.* [7], Breunung & Haller [8], Ponsioen *et al.* [9] and Jain & Haller [10]), the related computational tools assume a deterministic dynamical system. This assumption, however, does not hold for structures that are commonly subject to parameter uncertainties and external random disturbances.

The general relevance of a deterministic invariant manifold for the stochastically perturbed system can be investigated using, e.g. Monte Carlo methods (see Rubinstein & Kroese [11]). Due to their slow convergence, however, Monte Carlo methods require a high sample size, which leads to significant numerical costs. Furthermore, this numerical approach does not allow for a systematic understanding or general conclusions about qualitative aspects of the nonlinear dynamics.

The persistence of deterministic dynamical features, such as NHIMs or stable/centre manifolds of fixed points under random perturbations, is intricate to establish mathematically. Berglund & Gentz [12] studied a system with slow-fast dynamics and with a known slow manifold. They showed that under small external white noise excitation, sample paths remain close to the slow manifold with a certain probability for finite time. In a similar setting, Schmalfuss & Schneider [13] established the existence of a random invariant manifold, which eliminates the fast dynamics (also see Kuehn [14] for a summary). Both studies, however, assume an idealized, global slow-fast decomposition of variables into arbitrarily slow and fast variables, which is generally not available for realistic nonlinear mechanical systems.[1] Li *et al.* [16] removed this restriction and establish the persistence of NHIMs under random perturbation in a fairly general setting. However, they required the sample path of the random dynamical system to be close to trajectories of the deterministic counterpart in the C_1 norm, which is overly restrictive for the random noise models used in mechanics.

On the basis of linearization techniques by Wanner [17], Arnold [18] proved the existence of stable, unstable and centre manifolds of fixed points of random dynamical systems, both locally and globally. The conditions for the existence of global manifolds are restrictive, e.g. require the nonlinearity to be globally Lipschitz. The local invariant manifolds obtained from this analysis are non-unique as they depend on the choice of a cut-off function. Mohammed & Scheutzow [19] proved another stable manifold theorem for stochastic differential equations. Their result applies for certain nonlinearities with unbounded spatial derivatives. All these invariant manifolds and reduced models depend generally on the realization of the random process. Therefore, the computations leading to these individual reduced models can be computationally costly and do not immediately yield conclusions for the full random process.

By contrast, the probability density function, depending on position, velocity and time, is independent of the specific realizations of the random process. In the case of Gaussian white noise excitation, the time evolution of the probability density function is governed by the Fokker–Planck equation [20]. Its solution could, in principle, reveal the relevance of deterministic invariant manifolds for stochastically perturbed nonlinear mechanical systems. However, the exact steady-state solutions reported, e.g. by Caughey & Ma [21], Lin & Cai [22] and Soize [23] are inapplicable in practice since a peculiar relationship between the external white noise perturbations and the damping is required (Lin & Cai [22]). In the absence of exact solutions of the Fokker–Planck equation, approximate solutions have been constructed. For example,

[1] A slow-fast decomposition requires a peculiar scaling in the contraction rates. In the setting of nonlinear mechanical systems, contraction rates usually stem from the damping terms. The dissipative forces, however, are still not well understood and are challenging to identify (Kerschen *et al.* [15]). Thus, it can generally not be ensured that they are consistent with the mathematical theory. Indeed, Jain *et al.* [7] noticed the limitations of such slow-fast decomposition when applying a deterministic result to a finite element discretization of a von Kármán beam.

Atkinson [24] proposed an eigenfunction expansion or Ibrahim [25] or Crandall [26] obtained moment balance schemes by integrating the Fokker–Planck equation in space. Such methods, however, require a heuristic selection of truncation schemes or trial functions. More generally, the convergence of such methods is often unclear. Moreover, these approaches are computationally expensive, especially in higher dimensions (Soize [23]), and their numeric nature impedes general conclusions.

Structural engineers frequently use stochastic averaging or statistical linearization to assess the response of randomly excited nonlinear mechanical systems. Stochastic averaging, initially proposed by Stratonovich & Silverman [27], requires a transformation into a slowly varying amplitude equation. This transformation restricts the applications for the stochastic averaging techniques to primarily single-degree-of-freedom mechanical systems (Roberts & Spanos [28]). By contrast, statistical linearization (Roberts & Spanos [29]) was developed to handle systems with many degrees-of-freedom. It replaces the nonlinear dynamical system with a linear one implicitly assuming a Gaussian distribution for the response. The response of a nonlinear system to white noise, however, is usually non-Gaussian. Due to these limitations, these methods are unsuitable for clarifying the influence of noise on deterministic invariant manifolds.

In summary, the continued relevance of deterministic invariant manifolds under small random perturbations has not been well understood. As a consequence, the applicability of existing rigorous invariant manifold concepts to stochastically forced nonlinear mechanical systems has remained limited in practice. Moreover, numerical approaches for state space exploration tend to suffer from heuristic assumptions and high computational costs.

To address some of these issues, here, we apply tools derived by Haller *et al.* [30] to study diffusion in fluid flows. As Haller *et al.* [30] already noted, these tools can be applied to the Fokker–Planck equation governing the probability density function if the white noise has small intensity relative to the deterministic part of the system. Under that assumption, Haller *et al.* [30] identify diffusion barriers as material surfaces that extremize the diffusive transport of the probability density in the phase space. By the definition of these barriers, the transport of the probability density across them is purely driven by small stochastic perturbations of the otherwise deterministic system. Specifically, *perfect barriers* block the transport at leading order completely and thereby demarcate regions of the phase space that trajectories generally do not penetrate. Perfect barriers can be computed from purely deterministic quantities associated with the dynamical system, and hence computationally expensive numerical methods, such as Monte Carlo simulations, can be omitted.

We identify invariant manifolds of the limiting deterministic systems under small white noise excitation as barriers to the diffusive transport of the probability density function in the stochastic system. After transforming the Fokker–Planck equation to a suitable form, we extend the results of Haller *et al.* [30] to singular diffusion matrices, which unavoidably arise in mechanical systems[2] (§3). Thereafter, we study the asymptotic alignment of perfect barriers with SSMs and NHIMs in §4. Specifically, we prove that the transport of probability density across fast spectral submanifolds of the deterministic limit of the mechanical system is minimal at leading order, i.e. these manifolds act as perfect barriers for the probability density in the presence of small stochastic forcing. Furthermore, we show that the same conclusion holds for repelling NHIMs, which implies that hyperbolic slow manifolds act as barriers in backward time. We illustrate our results on specific nonlinear mechanical systems in §5.

[2]The underlying reason is that mechanical systems are customarily modelled by second-order differential equations and the Fokker–Planck equation requires a transformation to a first-order differential equation. This transformation extends the phase space by including velocities as coordinates. The velocities, however, are not forced by the stochastic terms and hence a singular diffusion matrix arises. We also note that the diffusion matrix $\mathbf{D}$ is given by $\mathbf{D} = \mathbf{B}\mathbf{B}^{\top}$ and refer to equation (2.5) where the null space is apparent.

2. Setup

We consider a model of a general nonlinear mechanical system of the form

$$\mathbf{M}\ddot{\mathbf{x}} + \mathbf{C}\dot{\mathbf{x}} + \mathbf{K}\mathbf{x} + \mathbf{S}_0(\mathbf{x}) + \mathbf{S}_1(\mathbf{x}, \boldsymbol{\Omega} t) = \sqrt{\nu}\mathbf{f}(\mathbf{x}, t), \quad 0 < \nu \ll 1, \ \ \mathbf{x}, \dot{\mathbf{x}} \in U \subset \mathbb{R}^N, \tag{2.1}$$

where $\mathbf{M}, \mathbf{C}$, and $\mathbf{K} \in \mathbb{R}^{N\times N}$ are the mass, stiffness and damping matrices and $\mathbf{x}(t)$ is the vector of generalized displacement variables. Equations (2.1) modelling a physical process are generally valid on a bounded domain, which we denote by U.

The function $\mathbf{S}_0(\mathbf{x}) = \mathcal{O}(|\mathbf{x}|^2)$ consists of autonomous nonlinear terms. The time-varying terms $\mathbf{S}_1(\mathbf{x}, \boldsymbol{\Omega} t)$ can include (nonlinear) parametric excitation as well as external forcing. The time dependence of $\mathbf{S}_1$ is assumed to be quasi-periodic with K incommensurate frequencies Ω_k, which includes the special cases of a steady ($K = 0$) and a time-periodic ($K = 1$) function $\mathbf{S}_1$. Moreover, we assume that $\mathbf{S}_0$ and $\mathbf{S}_1$ are at least five times continuously differentiable in space and $\mathbf{S}_1$ is at least continuously differentiable in time.

The right-hand side of equation (2.1) represents the stochastic excitation, with its differential defined as follows:

$$\mathrm{d}\mathbf{f}(\mathbf{x}, t) = \sum_{m=1}^{M} \mathbf{f}_m(\mathbf{x}, t)\, \mathrm{d}W_m, \quad m = 1, \ldots, M, \ \ M \geq 1, \tag{2.2}$$

where W_m are M uncorrelated Wiener processes. The vectors $\mathbf{f}_m(\mathbf{x}, t)$ specify the direction in which the white noise acts. We assume that the forcing directions $\mathbf{f}_m(\mathbf{x}, t)$ are continuous in space and time and bounded, which will be made more precise in the definition of a non-degenerate forcing matrix (see definition 4.1). In summary, the forcing in equation (2.1) can include external random forcing as well as random parametric forcing. Parametric random forcing has also been treated by Lin & Cai [22] and Soize [23], and such forcing has been observed in micro-electro-mechanical-systems (see Vig & Yoonkee [31] or Shoshani *et al.* [32]).

In this work, we establish the relevance of deterministic invariant manifolds for the stochastically perturbed nonlinear mechanical system (2.1). The connection between deterministic and stochastic dynamics is made via the Fokker–Planck equation governing the probability density function of system (2.1). Thus, we first introduce the Fokker–Planck equation for system (2.1). Subsequently, we briefly review SSMs and r-normally hyperbolic invariant manifolds (r-NHIMs). Due to their robustness both manifolds have been proven to be particularly relevant for analysing nonlinear dynamical systems, especially in the context of structural dynamics (cf. Jain *et al.* [7] and Haller & Ponsioen [6]).

(a) The Fokker–Planck equation of the nonlinear mechanical system (2.1)

To transform system (2.1) into an autonomous first-order form, we extend the phase space by letting

$$\mathbf{y} := \begin{bmatrix} \mathbf{x} \\ \dot{\mathbf{x}} \end{bmatrix} \in \mathbb{R}^{2N}, \tag{2.3}$$

and also define the velocity field

$$\mathbf{v}(\mathbf{y}, \boldsymbol{\Omega} t) := \begin{bmatrix} \dot{\mathbf{x}} \\ -\mathbf{M}^{-1}[\mathbf{K}\mathbf{x} + \mathbf{C}\dot{\mathbf{x}} + \mathbf{S}_0(\mathbf{x}) + \mathbf{S}_1(\mathbf{x}, \boldsymbol{\Omega} t)] \end{bmatrix} \in \mathbb{R}^{2N}. \tag{2.4}$$

To express the forcing (2.2) in the first-order formulation of system (2.1), we define the vectors

$$\mathbf{B}_m(\mathbf{x}, t) := \begin{bmatrix} \mathbf{0} \\ \mathbf{M}^{-1}\mathbf{f}_m(\mathbf{x}, t) \end{bmatrix} \in \mathbb{R}^{2N}, \quad m = 1, \ldots, M, \tag{2.5}$$

which point in the direction in which the mth Wiener process acts. Subsequently, we collect the directions (2.5) in the matrix

$$\mathbf{B} := [\mathbf{B}_1, \mathbf{B}_2, \ldots, \mathbf{B}_M] \in \mathbb{R}^{2N\times M}, \tag{2.6}$$

and define a m-dimensional vector consisting of one-dimensional Wiener processes:

$$\mathbf{W} = \begin{bmatrix} W_1 \\ W_2 \\ \vdots \\ W_M \end{bmatrix} \in \mathbb{R}^M. \tag{2.7}$$

With the velocity (2.4), the matrix (2.6) consisting of the directions of the stochastic perturbations (2.5) and the vector (2.7) of m Wiener processes, the phase space variables of system (2.1) are governed by the stochastic differential equation:

$$\mathrm{d}\boldsymbol{y} = \mathbf{v}\,\mathrm{d}t + \sqrt{\nu}\mathbf{B}(\mathbf{y}, t)\,\mathrm{d}\mathbf{W}, \quad 0 < \nu \ll 1, \tag{2.8}$$

where we have interpreted equation (2.1) in the sense of Itô (e.g. Williams *et al.* [33]). Our derivations are motivated by the nonlinear mechanical system (2.1); however, most of the following developments also apply for the more general, first-order system (2.8).

Alternatively, system (2.1) can be formulated as a stochastic differential equation utilizing the Stratonovich integral. By using Itô's integral formula, the Stratonovich formulation can be written as follows:

$$\mathrm{d}\boldsymbol{y} = \left[\mathbf{v}(\mathbf{y}, \boldsymbol{\Omega} t) + \frac{\sqrt{\nu}}{2}\sum_{m=1}^{M} \nabla(\mathbf{B}_m(\mathbf{y}, t))\mathbf{B}_m(\mathbf{y}, t)\right]\mathrm{d}t + \sqrt{\nu}\mathbf{B}(\mathbf{y}, t)d\mathbf{W}, \quad 0 < \nu \ll 1, \tag{2.9}$$

with an additional drift term (see Øksendal [34]). Calculating that additional term explicitly yields

$$\sum_{m=1}^{M} \nabla(\mathbf{B}_m(\mathbf{y}, t))\mathbf{B}_m(\mathbf{y}, t) = \sum_{m=1}^{M} \begin{bmatrix} \mathbf{0} & \mathbf{0} \\ \frac{\partial}{\partial \dot{\mathbf{x}}}\mathbf{M}^{-1}\mathbf{f}_m(\mathbf{x}, t) & \frac{\partial}{\partial \mathbf{x}}\mathbf{M}^{-1}\mathbf{f}_m(\mathbf{x}, t) \end{bmatrix} \begin{bmatrix} \mathbf{0} \\ \mathbf{M}^{-1}\mathbf{f}_m(\mathbf{x}, t) \end{bmatrix} = \mathbf{0}. \tag{2.10}$$

Thus, the Itô and the Stratonovich formulation of the mechanical system with white noise (2.1) are identical.

Hence, for both formulations, the probability density function $p(\mathbf{y}, t)$ satisfies the classic Fokker–Planck equation:

$$\frac{\partial p}{\partial t} + \nabla \cdot (p\mathbf{v}(\mathbf{y}, \boldsymbol{\Omega} t)) = \frac{\nu}{2}\nabla \cdot (\nabla \cdot (\mathbf{B}\mathbf{B}^{\top} p)), \quad p(\mathbf{y}_0, t_0) = p_0(\mathbf{y}_0), \tag{2.11}$$

where we have introduced the initial condition $p_0(\mathbf{y}_0)$. We assume that the mixed partial derivatives of the initial condition up to order two have a finite L_2-norm, which holds, e.g. for the Gaussian distribution. In the context of the Fokker–Planck equation (2.11), the velocity $\mathbf{v}(\mathbf{y}, \boldsymbol{\Omega} t)$ is often referred to as drift term (Risken [20]). The right-hand side of the Fokker–Planck equation (2.11) is denoted as diffusion term where the matrix $\mathbf{B}\mathbf{B}^{\top}$ is replaced by the diffusion matrix

$$\mathbf{D} := \mathbf{B}\mathbf{B}^{\top}. \tag{2.12}$$

Haller *et al.* [30] formulate their findings for fluid flows in a Lagrangian setting. To utilize these results, we introduce the Lagrangian or material derivative $Dp/Dt := p_t + (\nabla p)\mathbf{v}$ and rewrite the Fokker–Planck equation (2.11) in the following form:

$$\frac{Dp}{Dt} + p\nabla \cdot \mathbf{v} = \frac{\nu}{2}\nabla \cdot (\nabla \cdot (\mathbf{D}p)). \tag{2.13}$$

(b) Spectral submanifolds for the nonlinear mechanical system (2.1)

To precisely define SSMs for the mechanical system (2.1), we first note that the deterministic limit of system (2.8) is given by

$$\dot{\mathbf{y}} = \mathbf{v}(\mathbf{y}, \boldsymbol{\Omega} t). \tag{2.14}$$

For nonlinear oscillations, the time-dependent part of the vector field $\mathbf{S}_1(\mathbf{x}, \boldsymbol{\Omega} t)$ is often small, i.e. $\mathbf{S}_1(\mathbf{x}, \boldsymbol{\Omega} t) = \varepsilon\tilde{\mathbf{S}}_1(\mathbf{x}, \boldsymbol{\Omega} t)$ for some small parameter $\varepsilon > 0$ (cf. Haller & Ponsioen [6]). This mathematical necessity ensures that the linearization of system (2.16) remains influential for

the full nonlinear system. To transform the autonomous nonlinearities $\mathbf{S}_0(\mathbf{x})$ and the small non-autonomous terms $\varepsilon\tilde{\mathbf{S}}_1(\mathbf{x}, \boldsymbol{\Omega} t)$ into the first-order form, we introduce the following notation:

$$\mathbf{G}_0(\mathbf{x}) := \begin{bmatrix} \mathbf{0} \\ -\mathbf{M}^{-1}\mathbf{S}_0(\mathbf{x}) \end{bmatrix} \quad \text{and} \quad \mathbf{G}_1(\mathbf{x}, \boldsymbol{\Omega} t) := \begin{bmatrix} \mathbf{0} \\ -\mathbf{M}^{-1}\tilde{\mathbf{S}}_1(\mathbf{x}, \boldsymbol{\Omega} t). \end{bmatrix}. \tag{2.15}$$

With the definitions (2.15), equation (2.14) can be rewritten as follows:

$$\dot{\mathbf{y}} = \mathbf{A}\mathbf{y} + \mathbf{G}_0(\mathbf{y}) + \varepsilon\mathbf{G}_1(\mathbf{y}, \boldsymbol{\Omega} t), \quad 0 \leq \varepsilon \ll 1. \tag{2.16}$$

In the setting of equation (2.16), mechanical vibrations occur in the neighbourhood of the origin $\mathbf{y} = 0$, which is a stable fixed point of the autonomous limit of equation (2.16). To compute forced responses in the linear settings, mechanical engineers perform modal analysis, i.e. decouple the linearization of system (2.1) into N independent oscillators. Geometrically, this approach projects system (2.1) into invariant planes spanned by the eigenvectors of the linearization. Haller & Ponsioen [6] have precisely defined conditions under which the linear picture can be continued to the full nonlinear system. In this nonlinear setting, the invariant planes from the linearization deform into low-dimensional invariant submanifolds. Such SSMs have been proven to be valuable for model-order reduction (Haller & Ponsioen [6]), system identification (Szalai *et al.* [35]) and calculation of the forced response (Breunung & Haller [8]). Existence, robustness and uniqueness of SSMs can be established by the results of Haller & Ponsioen [6], which are based on more abstract results on invariant manifolds of Cabré *et al.* [36] and Haro & de la Lave [37].

To recall the results of Haller & Ponsioen [6], we label the eigenvalues of $\mathbf{A}$ by $\{\lambda_j\}_{1\leq j\leq 2N}$ and order them such that their real parts form the non-increasing sequence:

$$\mathrm{Re}(\lambda_{2N}) \leq \mathrm{Re}(\lambda_{2N-1}) \leq \cdots \leq \mathrm{Re}(\lambda_1) < 0. \tag{2.17}$$

As indicated in equation (2.17), the real parts of the eigenvalues λ_j are negative, since as previously mentioned the origin of the autonomous limit of equation (2.16) ($\varepsilon \to 0$) is assumed to be a stable fixed point. In the following, we consider invariant eigenspaces of the matrix $\mathbf{A}$, i.e. the autonomous ($\varepsilon \to 0$) linearization of equation (2.16) at the origin. We denote such an eigenspace by E and its dimension by $s := \dim(E)$. From the study by Haller & Ponsioen [6], we recall the definition of smooth nonlinear continuations of an eigenspace E as *spectral submanifolds*.

Definition 2.1. A SSM, $W(E)$, corresponding to an eigenspace E of the linear part is an invariant manifold of system (2.16) with the following properties:

(i) $W(E)$ has $s + K$ dimensions[3] and, for any fixed time t_0, the time-t_0 slice of $W(E)$ perturbs smoothly from E under the full nonlinear and $\mathcal{O}(\varepsilon)$ terms in system (2.16).
(ii) The manifold $W(E)$ is the smoothest among all invariant manifolds with property (i).

To restate the main theorem of Haller & Ponsioen [6], we introduce the spectral quotient $\Sigma(E)$ as follows:

$$\Sigma(E) := \mathrm{Int}\left(\frac{\min_{\lambda\in\mathrm{spect}(\mathbf{A})}(\mathrm{Re}(\lambda))}{\max_{\lambda\in\mathrm{spect}(\mathbf{A}|_E)}(\mathrm{Re}(\lambda))}\right), \tag{2.18}$$

where the function $\mathrm{Int}(\cdot)$ extracts the integer part of its argument. The spectral quotient (2.18) gives the quotient of the minimal real part of the eigenvalues λ_j and the maximal real part of

[3]Recall that K is the dimension of the frequency vector $\boldsymbol{\Omega}$.

all eigenvalues with their corresponding eigenspace included in the subspace E. The eigenvalues associated with the eigenspace E are *non-resonant*, if

$$\sum_{j=1}^{s} m_j \mathrm{Re}(\lambda_{q_j}) \neq \mathrm{Re}(\lambda_l), \quad \lambda_{q_j} \in \mathrm{spect}(\mathbf{A}|_E), \quad \lambda_l \notin \mathrm{spect}(\mathbf{A}|_E),$$

$$2 \leq \sum_{j=1}^{s} m_j \leq \Sigma(E), \quad m_j \in \mathbb{N}. \tag{2.19}$$

The non-resonance conditions (2.19) require that low-order linear combinations of the real parts of the eigenvalues with their corresponding eigenvector included in the linear subspace E are not equal to the real parts of the eigenvalues with their corresponding eigenvectors not included in E. We then have the following statement on the existence and persistence of SSMs of the unforced limit of general mechanical system (2.1).

Theorem 2.2. *Assume that the non-resonance conditions (2.19) are satisfied for an eigenspace E. Then*

1. *The SSM, $W(E)$, for system (2.16) uniquely exists in the class of $C^{\Sigma(E)+1}$ manifolds.*
2. *The SSM is robust with respect to smooth changes in parameters.*

Proof. This is a restatement of Haller & Ponsioen [6] deduced from more abstract results on invariant manifolds by Haro & de la Llave [37]. ∎

Remark 2.3 (Autonomous SSMs). The results from Haller & Ponsioen [6] are slightly stronger in the case that the deterministic system (2.16) is autonomous. The relevant spectral quotient is then defined as follows:

$$\sigma(E) := \mathrm{Int}\left(\frac{\min_{\lambda \in \mathrm{spect}(\mathbf{A}|) - \mathrm{spect}(\mathbf{A}|_E)}(\mathrm{Re}(\lambda))}{\max_{\lambda \in \mathrm{spect}(\mathbf{A}|_E)}(\mathrm{Re}(\lambda))} \right). \tag{2.20}$$

Comparing with the non-autonomous spectral quotient (2.18), the numerator of the autonomous spectral quotient (2.20) is restricted to eigenvalues with corresponding eigenvectors not included in E. The relevant non-resonance conditions are as follows:

$$\sum_{j=1}^{s} m_j \lambda_{q_j} \neq \lambda_l, \quad \lambda_{q_j} \in \mathrm{spect}(\mathbf{A}|_E), \lambda_l \notin \mathrm{spect}(\mathbf{A}|_E), \quad 2 \leq \sum_{j=1}^{s} m_j \leq \sigma(E), \; m_j \in \mathbb{N}. \tag{2.21}$$

The non-resonance conditions (2.21) depend on the eigenvalues λ_j and not just for the real part as in the non-autonomous case (cf. equation (2.19)). Thus, the non-resonance conditions for the autonomous case (2.21) are generally easier to satisfy than the resonance conditions in the non-autonomous case (2.19). The resulting SSM is time independent and tangent to the spectral subspace E at the origin. For more details on SSMs, we refer to Haller & Ponsioen [6].

(c) Normally hyperbolic invariant manifolds for the nonlinear mechanical system (2.1)

NHIMs, initially proposed by Fenichel [38], have been also been extensively discussed by Wiggins [2]. For an in-depth treatment, detailed derivations and specific characterizations of NHIMs, we refer to the aforementioned literature. Moreover, Jain *et al.* [7] apply NHIMs in the structural dynamics context.

The most crucial characteristics of NHIMs can be quantified in terms of their influence on vectors in their tangent and normal space (cf. figure 1). NHIMs are normally attracting in the sense that the normal component of vectors initially in the normal space shrink along NHIMs. Moreover, this attraction dominates any rate inside the tangent space by a factor of r. More specifically, vectors in the tangent space of a NHIM shrink or grow r times slower than normal components of normal vectors shrink. Hence, locally trajectories quickly settle on to the NHIM and lock on the slow flow inside the NHIM (cf. blue trajectories in figure 1)

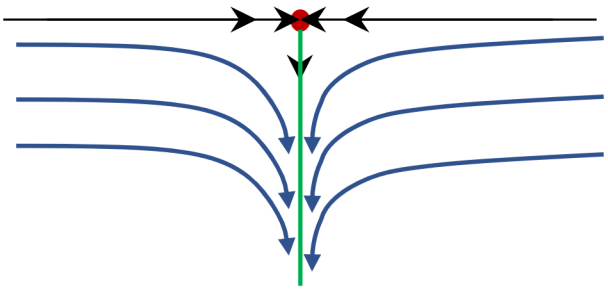

Figure 1. Sketch of a normally hyperbolic invariant manifold (green) emanating from a fixed point (red). The normal attraction rates dominate the tangential, slow flow. Typical trajectories in the neighbourhood of the NHIM are depicted in blue. (Online version in colour.)

3. Barriers to transport of the probability density $p(\mathbf{y}, t)$

In the following, we discuss barriers to the transport of diffusive scalars by a velocity field $\mathbf{v}$ and then refine the related results of Haller *et al.* [30] for mechanical vibrations. These results are stated for scalar concentrations fields governed by an advection-diffusion equation. Thus, we first recast the transformed Fokker–Planck equation (2.13) into advection-diffusion form. We start by noting that the divergence of the velocity (2.4) is given by the sum of the diagonal entries of the damping matrix $\tilde{\mathbf{C}} := \mathbf{M}^{-1}\mathbf{C}$, i.e.

$$\nabla \cdot \mathbf{v} = -\sum_{j=1}^{N} \tilde{C}_{jj} =: -c_0 = \text{const.} \tag{3.1}$$

Furthermore, we rewrite the right-hand side of equation (2.13) using the product rule of the divergence operator $\nabla \cdot (\mathbf{D}p) = p\nabla \cdot \mathbf{D} + \nabla(p)\mathbf{D}$. The divergence of the diffusion tensor $\mathbf{D}$ defined in equation (2.12) can be explicitly calculated to

$$\begin{aligned} \nabla \cdot \mathbf{D} &= \nabla \cdot \sum_{m=1}^{M} \mathbf{B}_m(\mathbf{x}, t)\mathbf{B}_m^{\top}(\mathbf{x}, t) = \sum_{m=1}^{M} \nabla \cdot \begin{bmatrix} \mathbf{0} & \mathbf{0} \\ \mathbf{0} & \mathbf{M}^{-1}\mathbf{f}_m(\mathbf{x}, t)\mathbf{f}_m^{\top}(\mathbf{x}, t)\mathbf{M}^{-\top} \end{bmatrix} \\ &= \sum_{m=1}^{M} \left[\mathbf{0}, \nabla_{\dot{\mathbf{x}}} \cdot \mathbf{M}^{-1}\mathbf{f}_m(\mathbf{x}, t)\mathbf{f}_m^{\top}(\mathbf{x}, t)\mathbf{M}^{-\top}\right] = \mathbf{0}, \end{aligned} \tag{3.2}$$

where $\nabla_{\dot{\mathbf{x}}}$ denotes the nabla operator restricted to the coordinates $\dot{\mathbf{x}}$. In summary, using equations (3.1) and (3.2), we recast equation (2.13) in the advection-diffusion form

$$\frac{\mathrm{D}p}{\mathrm{D}t} - c_0 p = \frac{\nu}{2}\nabla \cdot (\mathbf{D}\nabla p). \tag{3.3}$$

As previously mentioned, Haller *et al.* [30] work in a Lagrangian setting. To utilize this description, we introduce the deterministic flow map for system (2.14) by $\mathbf{F}_{t_0}^{t_1}(\mathbf{y}_0)$, which maps the initial conditions $\mathbf{y}_0$ to their later position $\mathbf{y}(t)$ at time t. Furthermore, the gradient of $\mathbf{F}_{t_0}^{t_1}(\mathbf{y}_0)$ with respect to the initial condition will be denoted by $\nabla_0 \mathbf{F}_{t_0}^{t}(\mathbf{y}_0)$. With this notation, Haller *et al.* [30] consider a material surface:

$$\mathcal{M}(t) = \mathbf{F}_{t_0}^{t}(\mathcal{M}_0). \tag{3.4}$$

The material surface $\mathcal{M}(t)$ is initially (at $t = t_0$) located at $\mathcal{M}_0$ and evolves under the flow of the velocity field $\mathbf{v}(\mathbf{y}, \boldsymbol{\Omega} t)$. The leading-order transport through the material surface $\mathcal{M}(t)$ can be

related to the transport tensor:

$$\begin{aligned}\mathbf{T}^t_{t_0}(\mathbf{y}_0) &:= \frac{1}{2}[\nabla_0\mathbf{F}^t_{t_0}(\mathbf{y}_0)]^{-1}\mathbf{D}(\mathbf{F}^t_{t_0}(\mathbf{y}_0),t)[\nabla_0\mathbf{F}^t_{t_0}(\mathbf{y}_0)]^{-\top}\\ &= \frac{1}{2}[\nabla_0\mathbf{F}^t_{t_0}(\mathbf{y}_0)]^{-1}\mathbf{B}(\mathbf{F}^t_{t_0}(\mathbf{y}_0),t)[(\nabla_0\mathbf{F}^t_{t_0}(\mathbf{y}_0))^{-1}\mathbf{B}(\mathbf{F}^t_{t_0}(\mathbf{y}_0),t)]^{\top}, \quad t > t_0 \in \mathbb{R}. \end{aligned} \tag{3.5}$$

Since the transport tensor is of fundamental importance for the upcoming derivations, we dissect it into its elements to understand its physical meaning. For each initial condition $\mathbf{y}_0 \in \mathcal{M}_0$ the matrix $\mathbf{B}(\mathbf{F}^t_{t_0}(\mathbf{y}_0),t)$ prescribes the directions of the Wiener processes at the time t and location $\mathbf{y}(t) = \mathbf{F}^t_{t_0}(\mathbf{y}_0) \in \mathcal{M}(t)$ inside the time-evolving material surface $\mathcal{M}(t)$. The inverse of the linearized flow map or the pullback operator $[\nabla_0\mathbf{F}^t_{t_0}(\mathbf{y}_0)]^{-1}$ acting on the directions $\mathbf{B}(\mathbf{F}^t_{t_0}(\mathbf{y}_0),t)$ (cf. the definition of the transport tensor (3.5)) transform these directions back to the initial position $\mathbf{y}_0$. Thus, left multiplying the matrix $[\nabla_0\mathbf{F}^t_{t_0}(\mathbf{y}_0)]^{-1}\mathbf{B}(\mathbf{F}^t_{t_0}(\mathbf{y}_0),t)$ with a vector $\mathbf{v}$ based at $\mathbf{y}_0$ yields an m-dimensional vector. Each entry indicates the strength of the direction $\mathbf{B}_m$ (cf. equation (2.5)) in the forward in time advected direction $\mathbf{v}(t) := \nabla_0\mathbf{F}^t_{t_0}(\mathbf{y}_0)\mathbf{v}_0$. The transport tensor (3.5) finally is the Gram matrix of the matrix $[\nabla_0\mathbf{F}^t_{t_0}(\mathbf{y}_0)]^{-1}\mathbf{B}(\mathbf{F}^t_{t_0}(\mathbf{y}_0),t)$. Hence, left and right multiplying it with two vectors $\mathbf{v}_0$ and $\mathbf{w}_0$ based at $\mathbf{y}_0$ yields a weighted scalar product of the two forward in time advected vectors $\nabla_0\mathbf{F}^t_{t_0}(\mathbf{y}_0)\mathbf{v}_0$ and $\nabla_0\mathbf{F}^t_{t_0}(\mathbf{y}_0)\mathbf{w}_0$. The weights of the weighted scalar product are determined by the diffusion matrix $\mathbf{D}(\mathbf{F}^t_{t_0}(\mathbf{y}_0),t)$ at the time t. In the following, the transport tensor (3.5) is utilized to measure the transport of the probability density $p(\mathbf{y},t)$ in the normal space of the material surface $\mathcal{M}(t)$.

While Haller *et al.* [30] assume a positive definite transport tensor, the tensor $\mathbf{D}$ defined in equation (3.2) does generally not have full rank (see equation (2.5)). Therefore, the transport tensor $\mathbf{T}^t_{t_0}(\mathbf{y}_0,t)$ in equation (3.5) is only positive semidefinite. Nevertheless, for the leading-order transport through, we can establish a result analogous to that of Haller *et al.* [30].

Theorem 3.1. *Over the time interval* $[t_0,t_1]$*, the total transport* $\Sigma^{t_1}_{t_0}$ *of the probability density* $p(\mathbf{y}_0,t)$ *through an arbitrary evolving material surface* $\mathcal{M}(t)$ *in the direction of one of its unit normal vectors* $\mathbf{n}_0(\mathbf{y}_0)$ *is given by*

$$\Sigma^{t_1}_{t_0}(\boldsymbol{n}_0) = \nu\int_{t_0}^{t_1}\int_{\mathcal{M}_0}\boldsymbol{n}_0^{\top}\boldsymbol{T}^t_{t_0}\nabla_0 p_0\,\mathrm{d}A\,\mathrm{d}t + \nu^p C(t_1), \quad \boldsymbol{n}_0 \in N_{\boldsymbol{y}_0}, \ \ |\boldsymbol{n}_0| = 1, \tag{3.6}$$

where $\mathrm{d}A$ *refers to the area element along* $\mathcal{M}_0$*;* $N_{\mathbf{y}_0}$ *denotes the normal space of* $\mathcal{M}_0$ *at the point* $\mathbf{y}_0$*;* $p > 1$ *and* $C(t_1)$ *denote constants depending on the time interval* $[t_0,t_1]$*.*

Proof. We detail the proof in Appendix A*a*. ∎

Remark 3.2. For arbitrarily large times t_1, there exists some (possibly small) ν such that the ν^2 terms in equation (3.6) are small compared with the leading order terms. Hence, theorem 3.1 allows us to study the leading-order transport for arbitrarily large time intervals, provided that the stochastic forcing can be chosen arbitrarily small.

From our earlier explanations, it follows that the transport $\Sigma^{t_1}_{t_0}(\mathbf{n}_0)$ defined in equation (A 7) sums diffusion weighted inner product of the forward in time advected normal vector $\mathbf{n}_0$ and the gradient of the initial condition $\nabla_0 p_0$ over the material surface $\mathcal{M}(t)$ and time interval $[t_0,t_1]$. The normal vector $\mathbf{n}_0$ and the gradient of the initial condition $\nabla_0 p_0$ are independent of time, and hence, the transport $\Sigma^{t_1}_{t_0}(\mathbf{n}_0)$ can be simplified by introducing the averaged transport tensor as follows:

$$\bar{\mathbf{T}}^{t_1}_{t_0}(\mathbf{y}_0) := \frac{1}{t_1 - t_0}\int_{t_0}^{t_1}\mathbf{T}^t_{t_0}(\mathbf{y}_0)\,\mathrm{d}t. \tag{3.7}$$

Then, following the arguments of Haller *et al.* [30], theorem 3.1 establishes that the largest possible, time averaged, leading-order diffusive transport through the material surface $\mathcal{M}_0$ is given by

$$\mathcal{E}(\mathcal{M}_0) = \frac{\int_{\mathcal{M}_0}\max_{\mathbf{n}_0\in N_{\mathbf{y}_0}\mathcal{M}_0,|\mathbf{n}_0|=1}|\mathbf{n}_0^{\top}(\mathbf{y}_0)\bar{\mathbf{T}}^{t_1}_{t_0}(\mathbf{y}_0)\nabla_0 p_0|dA_0}{\int_{\mathcal{M}_0}\mathrm{d}A_0}. \tag{3.8}$$

Taking the maximum in equation (3.8) ensures that the transport is indeed maximal. Expression (3.8) extends the results derived by Haller *et al.* [30] to positive semidefinite diffusion matrices $\mathbf{D}$ and material surfaces of arbitrary codimension.

Haller *et al.* [30] identify *perfect barriers* as codimension-one material surfaces completely blocking the diffusive transport at leading order. By equation (3.8), such perfect barriers in our setting satisfy the condition

$$\begin{aligned} &\langle \mathbf{n}_0(\mathbf{y}_0), \bar{\mathbf{T}}_{t_0}^{t_1}(\mathbf{y}_0)\nabla_0 p_0\rangle = \langle \bar{\mathbf{T}}_{t_0}^{t_1}(\mathbf{y}_0)\mathbf{n}_0(\mathbf{y}_0), \nabla_0 p_0\rangle = 0, \qquad \mathbf{y}_0 \in \mathcal{M}_0, \\ &\mathbf{n}_0(\mathbf{y}_0) \in N_{\mathbf{y}_0}\mathcal{M}_0, \ |\mathbf{n}_0(\mathbf{y}_0)| = 1. \end{aligned} \tag{3.9}$$

Condition (3.9) implies that the vector $\bar{\mathbf{T}}_{t_0}^{t_1}(\mathbf{y}_0)\nabla_0 p_0$ must be orthogonal to $\mathbf{n}_0(\mathbf{y}_0)$ or, equivalently, the vector $\bar{\mathbf{T}}_{t_0}^{t_1}(\mathbf{y}_0)\mathbf{n}(\mathbf{y}_0)$ orthogonal to the gradient of the initial condition $p_0(\mathbf{y}_0)$. Due to the lack of exact solutions to condition (3.9), numerical or approximative solutions have to be obtained (see Haller *et al.* [30]). If the norm of the transport tensor $\bar{\mathbf{T}}_{t_0}^{t_1}(\mathbf{y}_0)$ or initial gradient $\nabla_0 p_0(\mathbf{y}_0)$ is small, equation (3.9) is approximately satisfied by any choice for the normal vector $\mathbf{n}_0$. However, it is our interest to find surfaces such that their normal directions ensure locally minimal transport in the phase space. Therefore, we conclude that for approximate solutions and numerical simulations, the following normalized version of condition (3.9) is more suitable:

$$\mathbf{n}_0^\top(\mathbf{y}_0)\frac{\bar{\mathbf{T}}_{t_0}^{t_1}(\mathbf{y}_0)}{||\bar{\mathbf{T}}_{t_0}^{t_1}(\mathbf{y}_0)||}\frac{\nabla_0 p_0}{|\nabla_0 p_0|} = 0, \qquad \mathbf{y}_0 \in \mathcal{M}_0, \mathbf{n}_0(\mathbf{y}_0) \in N_{\mathbf{y}_0}\mathcal{M}_0, \ |\mathbf{n}_0(\mathbf{y}_0)| = 1. \tag{3.10}$$

Equation (3.10) is equivalent to condition (3.9) if the gradient of the initial condition p_0 is non-zero.

4. Alignment of barriers and invariant manifolds

In the following, we will investigate whether the condition (3.10) for perfect barriers are asymptotically met along invariant manifolds of the deterministic dynamical systems (2.14). Our first result gives conditions on an inflowing invariant manifold $\mathcal{M}_0$ of the deterministic system (2.14) to act as barriers under the addition of the small noise terms. Subsequently, we apply this result to two important classes of robust invariant manifolds, *r*NHIMs (cf. Fenichel [38]) and SSMs (cf. Haller & Ponsioen [6]).

We consider inflowing invariant manifolds $\mathcal{M}$, i.e. manifolds $\mathcal{M}$ that are forward time invariant for the flow map of the deterministic system (2.14). This requires that $\mathbf{F}_{t_0}^t(\mathcal{M}) \subset \mathcal{M}$ for all $t > t_0$ and that the velocity field (2.4) points strictly inward on the boundary $\partial\mathcal{M}$ for all times.

Along $\mathcal{M}$, we denote the tangent space of $\mathcal{M}$ at the point $\mathbf{y}(t) := \mathbf{F}_{t_0}^t(\mathbf{y}_0)$ by $T_{\mathbf{y}(t)}$ and the normal space by $N_{\mathbf{y}(t)}$. Furthermore, we define the orthogonal projections from the phase space $\mathbb{R}^{2N}$ into the normal and tangent space at point $\mathbf{y}(t)$ by

$$\Pi_{T_{\mathbf{y}(t)}\mathcal{M}} : \mathbb{R}^{2N} \mapsto T_{\mathbf{y}(t)}\mathcal{M}, \Pi_{N_{\mathbf{y}(t)}\mathcal{M}} : \mathbb{R}^{2N} \mapsto N_{\mathbf{y}(t)}\mathcal{M}, \quad \mathbf{y}(t) \in \mathcal{M}, \ \ t > t_0. \tag{4.1}$$

To quantify normal attraction or repulsion along $\mathcal{M}$, we follow the ideas of Fenichel [38] for inflowing invariant manifolds and define the linear mapping between normal spaces as follows:

$$\begin{aligned} &\mathbf{N}_{\mathbf{y}_0} : N_{\mathbf{y}}\mathcal{M} \to N_{\mathbf{y}_0}\mathcal{M}, \\ \text{and} \qquad &\Pi_{N_{\mathbf{y}_0}\mathcal{M}}[\nabla_0 \mathbf{F}_{t_0}^t(\mathbf{y}_0)]^{-1}\mathbf{w}_t \mapsto \mathbf{w}_0. \end{aligned} \tag{4.2}$$

In the mapping (4.2), the inverse of the linearized flow map $[\nabla_0 \mathbf{F}_{t_0}^t(\mathbf{y}_0)]^{-1}$ acting on the vector $\mathbf{w}_t$ inside the normal space at time t pulls this vector back to the initial position $\mathbf{y}_0$. Subsequently, the

projection $\Pi_{N_{\mathbf{y}_0}\mathcal{M}}$ ensures that the resulting vector is indeed in the normal space $\mathbf{N}_{\mathbf{y}_0}$. The norm of $N_{\mathbf{y}_0}$ quantifies normal expansion and contraction along $\mathcal{M}_0$, with its asymptotic limit given by *generalized Lyapunov number* (Fenichel [38])

$$\eta(\mathbf{y}_0) := \limsup_{t\to\infty} ||\mathbf{N}_{\mathbf{y}_0}(t)||^{1/(t-t_0)} = \limsup_{t\to\infty} \left(\max_{\mathbf{w}_t \in N_{\mathbf{y}(t)}} \frac{|\mathbf{N}_{\mathbf{y}_0}(t)\mathbf{w}_t|}{|\mathbf{w}_t|} \right). \tag{4.3}$$

We note that the generalized Lyapunov number is constant along trajectories and hence only depends on the forward limit set of $\mathcal{M}$ (Fenichel [38] or Wiggins [2]).

In addition, we define a Lyapunov-type exponent for the *full* backward time trajectory $\mathbf{F}_{t_1}^t(\mathbf{F}_{t_0}^{t_1}(\mathbf{y}_0))$ by

$$\mu_{max}(\mathbf{y}_0) := \limsup_{t\to\infty} \frac{1}{t-t_0} \log \left(\max_{\mathbf{u}\in\mathbb{R}^{2N}\setminus\{\mathbf{0}\}} \frac{|[\nabla_0 \mathbf{F}_{t_0}^t(\mathbf{y}_0)]^{-1}\mathbf{u}|}{|\mathbf{u}|} \right). \tag{4.4}$$

The aforementioned quantity provides an upper bound for the usual Lyapunov exponents:

$$\mu(\mathbf{y}_0, u) := \limsup_{t\to\infty} \frac{1}{t-t_0} \log \left(\frac{|[\nabla_0 \mathbf{F}_{t_0}^t(\mathbf{y}_0)]^{-1}\mathbf{u}|}{|\mathbf{u}|} \right). \tag{4.5}$$

For a detailed treatment of Lyapunov exponents, we refer to the studies by Chicone [39] or Oseledec [40]. Similar to the generalized Lyapunov numbers, the Lyapunov exponents and the Lyapunov type are constant along trajectories and only depend on the limit set of a family of trajectories.

We emphasize the lim sup in our definitions (4.3) and (4.4). Indeed, whether the limit of Lyapunov exponents in definition (4.5) exists is non-trivial, as shown by Oseledec multiplicative ergothic theorem [40]. Applying this theorem requires detailed knowledge about an invariant measure for the dynamical system (2.14), as Ott & Yorke [41] point out. In addition, they demonstrate on a nonlinear dynamical system that the limit of equation (4.5) does not exist in general.

To formulate our key technical lemma, let us introduce the notion of a *non-degenerate* forcing matrix $\mathbf{B}(\mathbf{F}_{t_0}^{t_1}(\mathbf{y}_0), t)$.

Definition 4.1. The forcing matrix $[\nabla_0 \mathbf{F}_{t_0}^t(\mathbf{y}_0)]^{-1}\mathbf{B}(\mathbf{F}_{t_0}^{t_1}(\mathbf{y}_0), t)$ is *non-degenerate* if the following two conditions are met.

1. The matrix $\mathbf{B}$ is bounded, i.e. there exists a constant $c_B > 0$ such that
$$||\mathbf{B}(\mathbf{x}, t)|| < c_B, \quad \mathbf{x} \in U, \quad t \in \mathbb{R}. \tag{4.6}$$
2. There exists a direction $\mathbf{u}^*(\mathbf{y}_0) \in \mathbb{R}^{2N}$ with $|\mathbf{u}^*(\mathbf{y}_0)| = 1$, a constant $C_B > 0$ and, for all $\mathbf{y}_0 \in \mathcal{M}_0$, there exists a time instant $t^*(\mathbf{y}_0) > t_0$ such that
$$\|(\mathbf{u}^*)^\top(\mathbf{y}_0)(\nabla_0 \mathbf{F}_{t_0}^t(\mathbf{y}_0))^{-1}\mathbf{B}(\mathbf{F}_{t_0}^t(\mathbf{y}_0), t)\| \geq C_B\, \mathrm{e}^{\mu_{\max}(\mathbf{y}_0)(t-t_0)} \quad t > t^*(\mathbf{y}_0), \text{ for all } \mathbf{y}_0 \in \mathcal{M}. \tag{4.7}$$

Remark 4.2. Let us remark that, if the trajectory $\mathbf{F}_{t_0}^t(\mathbf{y}_0)$ approaches a fixed point, $(\mathbf{u}^*)^\top$ denotes a projection into the direction with maximal backward time Lyapunov-type exponent and condition (4.7) requires the forcing $\mathbf{B}$ to excite this direction.

Equation (4.7) requires to advect the forcing $\mathbf{B}$ along the trajectory $\mathbf{F}_{t_1}^t(\mathbf{F}_{t_0}^{t_1}(\mathbf{y}_0))$ backwards to t_0. It suffices, however, to verify condition (4.7) along the forward time limit set in $\mathcal{M}(t)$. Moreover, we emphasize that equation (4.7) is purely deterministic and hence can be checked numerically without solving a stochastic system.

With the notion of the Lyapunov-type exponents (4.4) and the generalized Lyapunov-type number (4.3), we are now ready to state our technical main result.

Lemma 4.3. *Assume that there exists an inflowing invariant manifold $\mathcal{M}_0 \in U$ for the deterministic system* (2.14) *and assume that the forcing matrix $\mathbf{B}(\mathbf{F}_{t_0}^{t_1}(\mathbf{y}_0), t)$ is non-degenerate in the sense of definition 4.1. If the inequalities*

$$\log(\eta(\boldsymbol{y}_0)) < \mu_{\max}(\boldsymbol{y}_0), \quad \mu_{\max}(\boldsymbol{y}_0) > 0, \ \ \forall \boldsymbol{y}_0 \in \mathcal{M}_0, \tag{4.8}$$

hold, then $\mathcal{M}_0$ is asymptotically a perfect barrier, i.e. satisfies the perfect barrier condition (3.10) asymptotically as $t \to \infty$ for all $\mathbf{y}_0 \in \mathcal{M}_0$.

Proof. We detail the proof in Appendix A*b*. ■

Remark 4.4. The Lyapunov exponents and generalized Lyapunov numbers are constant along trajectories, and therefore, the condition of lemma 4.3 only needs to be verified at the forward time limit set of trajectories. The exponent $\mu_{\max}$ quantifies maximal growths or minimal shrinkage of perturbations to the trajectory $\mathbf{F}_{t_1}^{t}(\mathbf{F}_{t_0}^{t_1}(\mathbf{y}_0))$ in backward time. Therefore, condition (4.8) requires that perturbations at $\mathbf{F}_{t_0}^{t_1}(\mathbf{y}_0)$ in at least one direction grow as time marches backwards, i.e. decay in forward time. The number $\eta(\mathbf{y}_0)$ quantifies normal growth or shrinkage. In the case of normal repulsion in forward time, $\eta(\mathbf{y}_0)$ is smaller than one and hence its logarithm is negative. Therefore, condition (4.8) is satisfied, if $\mathcal{M}_0$ is either repelling ($\log(\eta(\mathbf{y}_0)) < 0$) or weakly attracting ($0 < \log(\eta(\mathbf{y}_0)) < |\mu_{\max}(\mathbf{y}_0)|$).

Remark 4.5. We have focused our derivations on the general mechanical system (2.1). Lemma 4.3, however, is more general. It applies to the diffusion of any scalar quantity, which can be modelled by the advection-diffusion equation (3.3).

Lemma 4.3 can be used to establish the relevance of various types of invariant manifolds of the deterministic system (2.14) under small stochastic excitations. Due to their robustness, *r*-NHIMs and SSMs have been proven to be particularly relevant for analysing nonlinear dynamical systems, especially in the context of structural dynamics (cf. Jain *et al.* [7] and Haller & Ponsioen [6]). The results on *r*-NHIMs, established by Fenichel [38], apply to compact inflowing invariant manifolds of the autonomous system (2.14). Based on remark 4.4 and the repelling nature of inflowing *r*-NHIMs, we expect the persistence of these *r*-NHIMs as perfect transport barriers. Indeed, applying lemma 4.3 to NHIMs, we obtain the following theorem.

Theorem 4.6. *Assume that there exists an inflowing, r-NHIM $\mathcal{M}$ with $\mu_{\max}(\mathbf{y}_0) > 0$ for the deterministic system* (2.14) *and the forcing matrix $\mathbf{B}(\mathbf{F}_{t_0}^{t_1}(\mathbf{y}_0), t)$ is non-degenerate in the sense of definition 4.1. Then, $\mathcal{M}$ is asymptotically a perfect barrier, i.e. satisfies the perfect barrier condition* (3.10) *asymptotically as $t \to \infty$ for all $\mathbf{y}_0 \in \mathcal{M}$.*

Proof. We detail the proof in Appendix A*c*. ■

Remark 4.7. By reversing time in theorem 4.6, we conclude that overflowing attracting NHIMs are barriers for the stochastically forced system (2.1), if the forcing directions are not degenerate. Overflowing and *r*-normally hyperbolic invariant provide a rigorous tool to reduce the dynamics of a nonlinear mechanical system to a slow manifold. Since overflowing *r*-NHIMs are inflowing *r*-NHIMs in backward time, theorem 4.6 establishes the relevance of these slow manifolds as diffusion barriers in backward time. A material surface minimizing transport in backward time maximizes the transport in forward time. Thereby, we conclude that attracting NHIMs are asymptotically transport maximizers. This confirms the intuition from the deterministic system for which trajectories are attracted to and accumulate on the NHIM. Intuitively, one would then expect that for small random perturbations it is very likely that a realization of the stochastic process penetrates the NHIM. With our derivations, we confirm that this deterministic intuition is indeed justified.

Remark 4.8. If $\mu_{\max}(\mathbf{y}_0)$ is negative along an *r*-NHIM, then the transport tensor $\bar{\mathbf{T}}_{t_0}^{t_1}(\mathbf{y}_0)$ decays towards zero, which implies that the unnormalized perfect barrier condition (3.9) holds. This is due to the fact that the integrand in definition (3.5) is bounded by a decaying exponential (see

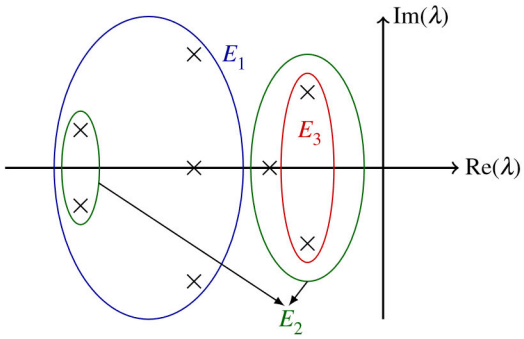

Figure 2. Possible eigenvalue configurations of the eigenspace E. The eigenvalues of E_1 and E_2 satisfy condition (4.9) of theorem 4.9, while E_3, the two-dimensional slow SSM, does not satisfy condition (4.9). (Online version in colour.)

the bounds (A 26) and (A 29) in Appendix A*b*). Therefore, the integral in equation (3.7) is upper-bounded by a constant and vanishes after taking the time average. Therefore, an r-NHIM with $\mu_{\max}(\mathbf{y}_0) < 0$ satisfies equation (3.9) asymptotically as $t \to \infty$ for all $\mathbf{y}_0 \in \mathcal{M}_0$.

For the autonomous case (i.e. $\varepsilon = 0$ in equation (2.16)), we apply lemma 4.3 to an SSM, $W(E)$, tangent to the subspace E and obtain the following.

Theorem 4.9. *Assume that the deterministic system* (2.16) *is autonomous, the non-resonance conditions* (2.21) *are satisfied for an eigenspace E of the origin (i.e. the SSM exists) and that the forcing matrix* $\mathbf{B}(\mathbf{0}, t)$ *is non-degenerate (cf. definition 4.1). If all directions not included, E decays slower than the fastest decay rate, i.e.*

$$\mathrm{Re}(\lambda_{2N}) < \min_{\lambda \in \mathrm{spect}(A) - \mathrm{spect}(A|_E)} \mathrm{Re}(\lambda), \tag{4.9}$$

then the SSM $W(E)$ *is asymptotically a perfect barrier, i.e. satisfies the perfect barrier condition* (3.10) *asymptotically as* $t \to \infty$ *for all* $\mathbf{y}_0 \in \mathcal{M}_0$.

Proof. We apply lemma 4.3 to points inside the stable manifold of the origin. We detail the derivations in Appendix A*d*. ∎

To illustrate condition (4.9), we sketch the possible eigenvalue configuration in figure 2. Fast SSMs of arbitrary dimension (e.g. $W(E_1)$ in figure 2) satisfy the condition (4.9) of theorem 4.9. The intermediate SSM $W(E_2)$ depicted in figure 2 also satisfies condition (4.9) since the fastest decaying directions are included in the subspace E_s. For the two-dimensional slow SSM, $W(E_3)$ condition (4.9) is not satisfied.

Remark 4.10 (non-autonomous systems). Theorem 4.9 can be extended to the non-autonomous setting (i.e. $\varepsilon > 0$ in equation (2.16)) as well. Compared with our derivations in Appendix A*d*, the forward time limit set will be a quasi-periodic orbit $\mathbf{y}_\varepsilon$, for which the numbers $\eta(\mathbf{y}_\varepsilon)$ and $\mu_{\max}(\mathbf{y}_\varepsilon)$ need to be computed. For small $\varepsilon > 0$, the quasi-periodic orbit $\mathbf{y}_\varepsilon$ is normally hyperbolic, and thus by the persistence of the Lyapunov-type numbers established by Fenichel [38], $\eta(\mathbf{y}_\varepsilon)$ and $\mu_{\max}(\mathbf{y}_\varepsilon)$ are $\mathcal{O}(\varepsilon)$ close to their values evaluated for the autonomous limit $\varepsilon \to 0$. For the autonomous limit $\varepsilon \to 0$, the quasi-periodic orbit is the origin for which $\eta(\mathbf{0})$ and $\mu(\mathbf{0})$ can be computed explicitly (cf. Appendix A*d*). Thus, if the autonomous limit of equation (2.16) satisfies the assumptions of theorem (d), then the SSM $W(E)$ for the non-autonomous system is asymptotically a perfect barrier.

5. Numerical examples

In the following, we verify our theoretical findings from §4 and demonstrate numerically that deterministic manifolds are of continued relevance under small stochastic excitation. As proven in

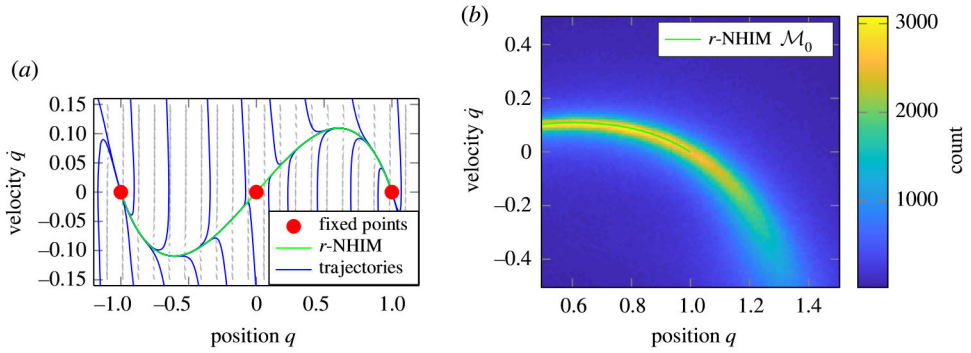

Figure 3. Phase space of the autonomous limit of system (5.1) and sampled phase space for the numerical investigations. (*a*) Fixed points and heteroclinic connection of system (5.1) with the parameters (5.2). (*b*) *r*-NHIM and counting variable for 10^6 realizations of equation (5.1). (Online version in colour.)

§4, r-NHIMs and fast SSMs can serve as perfect barriers for the stochastically excited mechanical system. For illustrative purposes, we start with the classical Duffing oscillator. Subsequently, we proceed to an example with two degrees-of-freedom (i.e. four dimensions).

(a) Duffing oscillator

We illustrate the relevance of *r*-NHIMs and fast SSMS as barriers on the stochastically excited classical Duffing oscillator

$$\ddot{q} + c\dot{q} + kq + \kappa q^3 = \sqrt{\nu} f, \quad \int_{t_0}^{t} f \, \mathrm{d}t = \int_{0}^{t} \mathrm{d}W, \tag{5.1}$$

with parameters

$$c = 3.5, \quad k = -1, \quad \kappa = 1. \tag{5.2}$$

The autonomous limit of system (5.1) has two stable fixed points at $\dot{q} = 0$ and $q = \pm 1$ and a saddle type fixed point at $\dot{q} = q = 0$. The unstable manifold of the saddle at the origin connects to the slow stable direction of the two other fixed points (cf. figure 3*a*). This heteroclinic connection is an attracting NHIM, which we denote by $\mathcal{M}_0$. In backward time, the maximal Lyapunov exponent of all trajectories inside $\mathcal{M}_0$ is given by the negative decay rate at the saddle point, which is positive. The forcing vector of the phase space equivalent of system (5.1), see also equation (2.5), is not orthogonal to the decaying direction at the fixed saddle point and hence the forcing is non-degenerate. Therefore, theorem 4.6 together with remark 4.7 applies and we expect maximal transport across $\mathcal{M}_0$.

Setting $\sqrt{\nu} = 0.01$, we simulate 10^6 realizations of the stochastic system (5.1) for $t_1 = 10$ time units with the forward Euler scheme. Moreover, we draw the initial condition from a Gaussian distribution centred at the stable fixed point $q = 1$ with a standard deviation of one. Since $\mathcal{M}_0$ enables transport of the probability density, it also maximizes the crossing of realizations of the random process (5.1). Therefore, we expect that trajectories of the random process (5.1) accumulate at $\mathcal{M}_0$. To demonstrate an accumulation of trajectories, we discretize time and phase space of system (5.1). We divide the phase space into boxes and count the number of realizations in a given box for a given time instance. By summing this number for all time instances, we obtain a counting variable for each box, which we depict in figure 3*b*. As predicted by theorem 4.6, trajectories often cross $\mathcal{M}_0$ and therefore they stay close to $\mathcal{M}_0$.

For the forward time direction, there exists a fast SSM tangent to the fast decaying direction of the stable fixed point at $q = 1$. According to theorem 4.9, the transport of probability density across this fast SSM is minimal. To demonstrate minimal transport, we search the phase space of system (5.1) for a barrier with minimal transport numerically. We start by attaching a small line

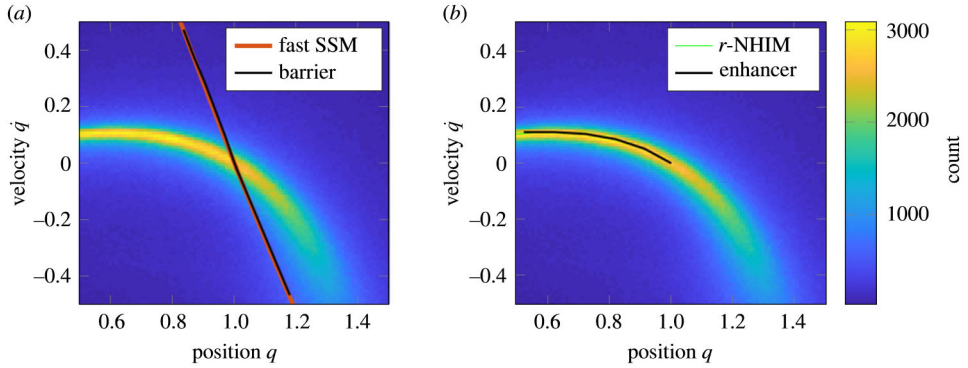

Figure 4. Fast SSM, *r*-NHIM and numerically identified barriers for the Duffing oscillator (5.1), with small intensity $\sqrt{\nu} = 0.01$. (*a*) Fast SSM and numerically identified barrier with minimal transport and (*b*) *r*-NHIM and numerically identified enhancer with maximal transport. (Online version in colour.)

segment with a fixed length to the fixed point and vary the position of the end point of the line segment such that the number of realizations crossing this line is minimal. Having found such a line, we iteratively grow the barrier by attaching a new line segment to the end of the barrier such that the number of realizations crossing the new line segment is again minimal.

We depict the identified line with minimal transport in figure 4*a* and observe a close match with the fast SSM as predicted by theorem 4.9. Numerically searching for a enhancer with maximal number of trajectory crossings in a similar manner, we obtain the black curve in figure 4*b*. The enhancer with maximal number of trajectory crossings aligns closely with the *r*-NHIM as predicted by theorem 4.6.

Throughout our derivations, we rely on the fact that the stochastic terms are small. In system (2.1), this smallness is expressed by the small parameter $\sqrt{\nu}$ scaling the noise terms. To stress the importance of this assumption, we increase the parameter $\sqrt{\nu}$ to 0.1, repeat our investigations for the Duffing oscillator (5.1) and depict our results in figure 5. Similar to the case with a smaller $\sqrt{\nu}$, the counting variable is high close to the *r*-NHIM. Thus, trajectories are still attracted to the NHIM. However, frequently visited phase space locations, indicated by a high counting variable, are more distant to the NHIM compared with the case with smaller noise intensity (cf. figure 4). This is expected as the stronger stochastic perturbation can induce larger deviations from the attracting *r*-NHIM. Moreover, the numerically identified barrier with maximal crossings starts to deviate from the *r*-NHIM and, similarly, the barrier with minimal crossings departs from the fast SSM. This indicates that the applicability of our theorems 4.6 and 4.9, based on the assumption of small noise terms, deteriorates. However, even for the noise intensity $\sqrt{\nu} = 0.1$ barriers with maximal and minimal crossings are still in the general vicinity of the deterministic invariant manifolds. We expect that for increasing noise intensities, this misalignment will generally grow.

(b) Multi-dimensional example

As an mechanical system with a *r*-NHIM, we select an extension of the single-degree-of-freedom Duffing oscillator (5.1) of the form

$$\ddot{\mathbf{q}} + \begin{bmatrix} c & 0 \\ 0 & c \end{bmatrix} + \dot{\mathbf{q}} \begin{bmatrix} k+\varepsilon & -\varepsilon \\ -\varepsilon & k+\varepsilon \end{bmatrix} \mathbf{q} + \begin{bmatrix} \kappa q_1^3 \\ \kappa q_2^3 \end{bmatrix} = \begin{bmatrix} 0 \\ \sqrt{\nu} \end{bmatrix} f, \quad \int_0^t f \, \mathrm{d}t = \int_{t_0}^t \mathrm{d}W, \tag{5.3}$$

where the random excitation acts on the second degree-of-freedom only. The coupling stiffness ε is assumed to be small.

For the limit $\varepsilon \to 0$, both degrees of freedom are decoupled and their phase space is structured, as depicted in figure 3*a*. This implies that in the phase space of each degree of freedom individually, there exists a one-dimensional *r*-NHIM. From this geometry, we conclude that inside

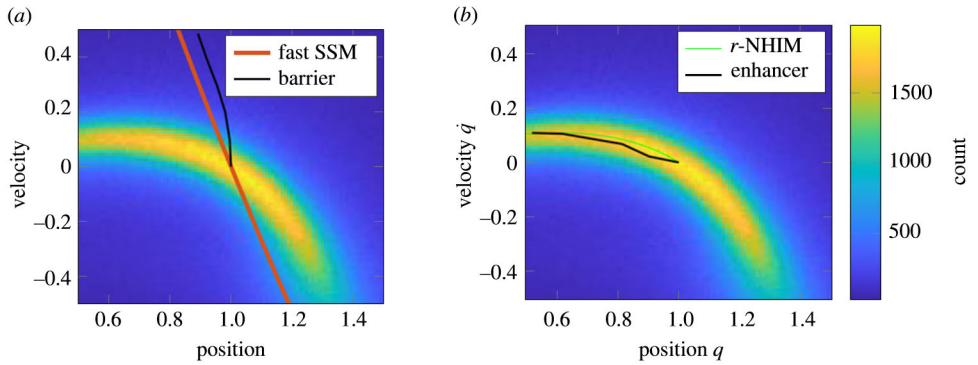

Figure 5. Fast SSM, *r*-NHIM and numerically identified barriers for the Duffing oscillator (5.1) with larger noise intensity $\sqrt{\nu} = 0.1$. (*a*) Fast SSM and numerically identified barrier with minimal transport and (*b*) *r*-NHIM and numerically identified enhancer with maximal transport. (Online version in colour.)

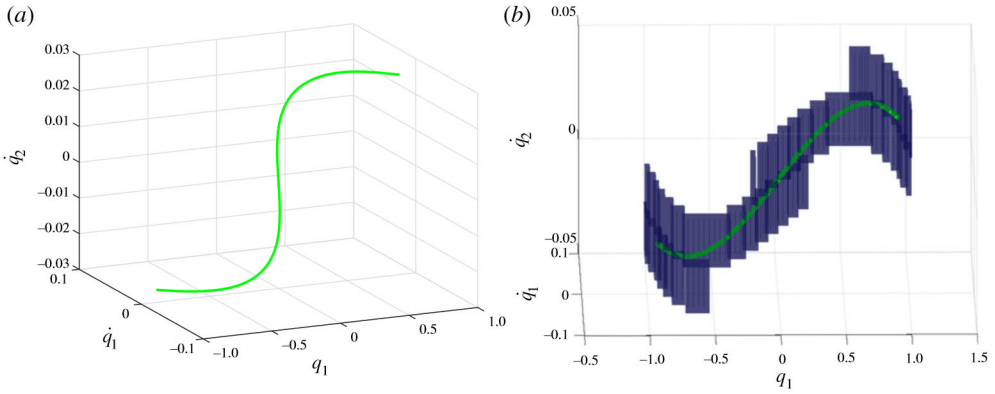

Figure 6. Slow manifold and frequently visited phase space locations inside the trap $q_2 = 0$. (*a*) Intersection of slow manifold and the hyperplane $q_2 = 0$, (*b*) slow manifold (green) and the 200 most frequently visited phase space locations inside the hyperplane $q_2 = 0$. (Online version in colour.)

the four-dimensional phase space, there is a two-dimensional *r*-NHIM for the limit $\varepsilon \to 0$. Since *r*-NHIMs are robust to smooth perturbations (Fenichel [38]), the two-dimensional *r*-NHIM survives for small values of ε. In the following, we select $\varepsilon = 0.1$ and the parameters (5.2).

To compute an approximation of the two-dimensional slow manifold, we initialize trajectories close to the saddle equilibrium at the origin. Since the origin is on the slow manifold and the r-NHIM is attracting, we infer that trajectories will closely follow the slow manifold. Thereby, these trajectories serve as a good approximation of the *r*-NHIM. We obtain these trajectories by numerically integrating system (5.3) without stochastic load (i.e. $\nu \to 0$). Subsequently fitting a surface through these trajectories, we obtain an approximation of the slow manifold. Since the *r*-NHIM is embedded in a four-dimensional space, it can only be displayed by taking appropriate cross sections or projections. We depict the cross section of the slow manifold with the hyperplane $q_2 = 0$ in figure 6*a*.

Similar to §(a), we simulate 10^6 realizations of the random dynamical system (5.3) for $t_1 = 10$ time units with the forward Euler scheme. Once again, we draw the initial condition from a Gaussian distribution centred at the stable fixed point $q_1 = q_2 = 1$ with a standard deviation of one and set $\sqrt{\nu} = 0.01$. By the transport enhancing property of the *r*-NHIM predicted by theorem 4.6 and remark 4.7, we expect trajectories to stay close to the slow manifold. To verify this

numerically, we calculate the counting variable, as described in §(a), inside the three-dimensional hyperplane $q_2 = 0$ on a three-dimensional grid. In this case, the counting variable cannot be easily visualized by an intensity plot. Therefore, we choose to colour the 200 phase space volumes with the highest value of the counting variable inside the trap blue in figure 6*b*. As predicted by theorem 4.6 and remark 4.7, trajectories concentrate close to the *r*-NHIM.

6. Conclusions

We have shown that deterministic invariant manifolds of general nonlinear mechanical systems are of continued relevance if small, white noise perturbations are added. To this end, we have applied and extended the concept of diffusion barriers from fluid mechanics, which are material surfaces minimizing diffusive transport (Haller *et al.* [30]), to stochastically excited nonlinear mechanical systems. Our results reveal that fast SSMs and *r*-normally hyperbolic invariant manifolds, two important and robust invariant manifolds for applications in dynamical systems, asymptotically serve as diffusion barriers. From the transport-hindering character of these surfaces, we conclude that these objects demarcate phase space regions that trajectories of the random dynamical system generally do not penetrate.

We obtain that spectral submanifolds associated with a stable equilibrium generally serve as asymptotic barriers to diffusive transport, unless the slowest decaying directions are included in the SSM. This indicates that these SSMs, initially proposed for model-order reduction of deterministic systems, remain relevant under the addition of small white noise terms. Specifically they are observable in a more realistic, experimental setting. We illustrate the asymptotic alignment of perfect barriers with a fast SSM on an explicit numerical example.

The alignment of repelling *r*-normally hyperbolic invariant manifolds and perfect barriers establishes the relevance of slow manifolds as diffusion barriers in backward time. Thereby, the deterministic phase space geometry of a slow manifold as a strongly repelling structure in backward time is robust with respect to small, white noise perturbations. Since slow SSMs can be *r*-NHIMs for the reversed-time flow, the robustness of *r*-NHIMs can also establish the continued relevance of slow SSMs as asymptotic diffusion barriers for the stochastically perturbed system.

Our analytical treatment reveals the importance of fast SSMs and *r*-normally hyperbolic invariant manifolds without the use of numerics. This enables an extension of the deterministic phase space geometry to the stochastic setting, without relying on extensive numerics such as Monte Carlo sampling.

As future continuation of our analysis, we envision an extension to extract information about the steady-state response of nonlinear mechanical systems subject to small white noise excitation. Indeed, in engineering applications, the steady-state response of the mechanical systems is an important design criterion and performance indicator.

Data accessibility. Software code to reproduce the numerical investigations of §5 is publicly available at https://github.com/tbreunung/Barriers_for_RandomVib.

Authors' contributions. T.B.: formal analysis, investigation, methodology, software, validation, visualization, writing—original draft, writing—review and editing; F.K.: investigation, validation, writing—review and editing; G.H.: conceptualization, funding acquisition, project administration, supervision, writing—review and editing.

All authors gave final approval for publication and agreed to be held accountable for the work performed therein.

Conflict of interest declaration. We declare we have no competing interests.

Funding. We received no funding for this study.

Acknowledgements. We are grateful to Bálint Kaszás for raising our attention towards Stratonovich's interpretation of a stochastic integral. T.B. is also thankful to Themistoklis Sapsis and Keith Worden for introductory and fruitful discussions on random dynamical systems and encouragement to work in this field, respectively.

Appendix A

(a) Proof of theorem 3.1

To prove theorem 3.1, we follow the derivations of Haller *et al.* [30] and consider the rate of change of probability density in an enclosed volume:

$$\frac{\mathrm{d}}{\mathrm{d}t}\int_{V(t)} p(\mathbf{y},t)\,\mathrm{d}V = \frac{\mathrm{d}}{\mathrm{d}t}\int_{V_0} p(\mathbf{F}_{t_0}^t(\mathbf{y}_0),t)\det(\nabla_0\mathbf{F}_{t_0}^t(\mathbf{y}_0,t))\,\mathrm{d}V_0. \tag{A 1}$$

Liouville's formula (cf. Chicone [39]) gives

$$\det(\nabla_0\mathbf{F}_{t_0}^t(\mathbf{y}_0,t)) = \exp\left(\int_{t_0}^t \nabla\cdot\mathbf{v}(\mathbf{F}_{t_0}^s(\mathbf{y}_0),\boldsymbol{\Omega}s)ds\right) = \mathrm{e}^{-c_0(t-t_0)}, \tag{A 2}$$

where we have used the divergence of the mechanical system (3.1). Denoting the probability density $\hat{p}(\mathbf{y}_0,t) := p(\mathbf{F}_{t_0}^t(\mathbf{y}_0),t)$ in Lagrangian coordinates, we transform equation (A 1) to Lagrangian coordinates yielding

$$\frac{\mathrm{d}}{\mathrm{d}t}\int_{V(t)} p(\mathbf{y},t)\,\mathrm{d}V = \int_{V_0}[\partial_t\hat{p}(\mathbf{y}_0,t) - c_0\hat{p}(\mathbf{y}_0,t)]\mathrm{e}^{-c_0(t-t_0)}\,\mathrm{d}V_0. \tag{A 3}$$

To transform the advection-diffusion equation (3.3) into Lagrangian coordinates, we use the explicit formulas of Tang and Boozer [42] as well as Thiffeault [43],

$$\partial_t\hat{p}(\mathbf{y}_0,t) - c_0\hat{p}(\mathbf{y}_0,t) = \nu\nabla_0\cdot(\mathbf{T}_{t_0}^t\nabla_0\hat{p}(\mathbf{y}_0,t)). \tag{A 4}$$

Taking the time derivative of the variable $\hat{\mu}(\mathbf{y}_0,t) := \mathrm{e}^{-c_0(t-t_0))}\hat{p}(\mathbf{y}_0,t)$ yields

$$\begin{aligned}\partial_t\hat{\mu}(\mathbf{y}_0,t) &= (\partial_t\hat{p}(\mathbf{y}_0,t) - c_0\hat{p}(\mathbf{y}_0,t))\mathrm{e}^{-c_0(t-t_0))} = \nu\nabla_0\cdot(\mathbf{T}_{t_0}^t\nabla_0\,\mathrm{e}^{-c_0(t-t_0))}\hat{p}(\mathbf{y}_0,t))\\ &= \nu\nabla_0\cdot(\mathbf{T}_{t_0}^t\nabla_0\hat{\mu}(\mathbf{y}_0,t)).\end{aligned} \tag{A 5}$$

With equation (A 5), we rewrite the rate of change of probability density in phase a space volume (A 3) as follows:

$$\begin{aligned}\frac{\mathrm{d}}{\mathrm{d}t}\int_{V(t)} p(\mathbf{y},t)\,\mathrm{d}V &= \int_{V_0}\nu\nabla_0\cdot(\mathbf{T}_{t_0}^t\nabla_0\hat{\mu}(\mathbf{y}_0,t))\mathrm{d}V_0\\ &= \int_{\partial V_0}\nu\langle\mathbf{D}\nabla_0\hat{\mu}(\mathbf{y}_0,t),\mathbf{n}(\mathbf{y}(t))\rangle\,\mathrm{d}A_0,\end{aligned} \tag{A 6}$$

where we have used the divergence theorem and the last integral denote the surface integral over the $2N-1$ dimensional boundary $\partial V(t)$ of the $2N$ dimensional volume $V(t)$.

In the following, we show that the arguments from Haler *et al.* [30] can be extended to account for surfaces with codimension higher than one. For any material surface $\mathcal{M}_0$, we can select a volume V_0 such that the material surface $\mathcal{M}_0$ is part of the boundary of V_0. Then, the total flux over the boundary of $V(t) = \mathbf{F}_{t_0}^t(V_0)$ is given by the integral (A 6). The total flux through the boundary ∂V_0 can be written as a summation over subsets of ∂V_0. Thereby the individual contribution of the subset $\mathcal{M}(t)\subset\partial V(t)$ to the total flux over the time interval $[t_0,t_1]$ is given by

$$\Sigma_{t_0}^{t_1}(\mathcal{M}_0,N\mathcal{M}_0) := \nu\int_{t_0}^{t_1}\int_{\mathcal{M}_0}\langle\mathbf{T}_{t_0}^t\nabla_0\hat{p}(\mathbf{y}_0,t),\mathbf{n}(\mathbf{y}_0)\rangle\,\mathrm{d}A\,\mathrm{d}t,\quad \mathbf{n}(\mathbf{y}_0)\in N_{\mathbf{y}_0}\mathcal{M}(t). \tag{A 7}$$

Contrary to Haller *et al.* [30], our formula (A 7) depends on the specific choice of unit normal vectors inside the normal bundle $N\mathcal{M}(t)$.

Taking the gradient of equation (A 5) as an integrate in time, we obtain

$$\nabla_0\hat{\mu}(\mathbf{y}_0,t)=\nabla_0 p(\mathbf{y}_0)+\nu\int_{t_0}^{t}\nabla_0[\nabla_0\cdot(\mathbf{T}_{t_0}^{s}\nabla_0\hat{\mu}(\mathbf{y}_0,s))]\mathrm{d}s, \tag{A 8}$$

where we have used that $\nabla_0\hat{\mu}(\mathbf{y}_0,t_0)=\nabla_0 p(\mathbf{y}_0)$. With equation (A 8), the flux vector (A 7) can be expressed as follows:

$$\begin{aligned}\Sigma_{t_0}^{t_1}(\mathcal{M}_0,N\mathcal{M}_0)=\nu&\int_{t_0}^{t_1}\int_{\mathcal{M}_0}\langle\mathbf{T}_{t_0}^{t}\nabla_0 p(\mathbf{y}_0),\mathbf{n}(\mathbf{y}_0)\rangle\,\mathrm{d}A_0\,\mathrm{d}t\\&+\nu^2\int_{t_0}^{t_1}\int_{\mathcal{M}_0}\int_{t_0}^{t}\langle\mathbf{T}_{t_0}^{t}\nabla_0[\nabla_0\cdot(\mathbf{T}_{t_0}^{s}\nabla_0\hat{\mu}(\mathbf{y}_0,s))],\mathbf{n}(\mathbf{y}_0)\rangle\,\mathrm{d}A_0\,\mathrm{d}s\,\mathrm{d}t.\end{aligned} \tag{A 9}$$

Then, the transport of the probability density $p(\mathbf{y}_0,t)$ through an arbitrary surface $\mathcal{M}(t_0)$ into the normal direction $\mathbf{n}_0$ can be written as (3.6) if the solution to the initial value problem

$$\left.\begin{aligned}\frac{\partial\hat{\mu}}{\partial t}&=\nu\nabla_0\cdot(\mathbf{T}_{t_0}^{t}(\mathbf{y}_0)\nabla_0\hat{\mu}(\mathbf{y}_0,t)),\\ \text{and}\qquad\hat{\mu}(\mathbf{y}_0,t_0)&=p_0,\end{aligned}\right\} \tag{A 10}$$

satisfies

$$\sup_{\mathbf{y}_0\in U,\,t_0\le t\le t_1}|\nabla_0\hat{\mu}(\mathbf{y}_0,t)-\nabla_0 p(\mathbf{y}_0)|=\mathcal{O}(\nu^q), \tag{A 11}$$

for some $q>0$. Indeed, using equation (A 10), integrating the t-derivative by the Fundamental Theorem of Calculus and estimating by the supremum in $\mathbf{x}_0$ and t give condition (A 11) To establish equation (A 11), Haller *et al.* [30] assume a positive definite transport tensor. In our application, however, the matrix $\mathbf{D}=\mathbf{B}\mathbf{B}^{\top}$ is not of full rank and therefore the transport tensor (3.5) is only positive-semidefinite. Defining $\xi(t):=\hat{\mu}(\mathbf{y}_0,t)-p(\mathbf{y}_0)$, we transform equation (A 10) to

$$\left.\begin{aligned}\frac{\partial\xi}{\partial t}&=\nu\nabla_0\cdot(\mathbf{T}_{t_0}^{t}(\mathbf{y}_0)\nabla_0(\xi(\mathbf{y}_0,t)+p(\mathbf{y}_0)))\\ \text{and}\qquad\xi(\mathbf{y}_0,t_0)&=0.\end{aligned}\right\} \tag{A 12}$$

For positive semidefinite diffusion tensors, we use an estimate by Igari [44] for solutions to degenerate parabolic equations, which we restate in our setting:

Lemma A.1. *Let $\hat{\mu}$ be a solution to equation* (A 10) *and assume that $\mathbf{T}_{t_0}^{t}(\mathbf{y}_0)$ and $\nabla_0 p(\mathbf{y}_0)$ are sufficiently regular. Then, for $m\ge 0$, the upper bound*

$$||\xi(t)||_{H^m(U)}\le\int_{t_0}^{t}\mathrm{e}^{\nu\gamma(t-s)}||\nu\nabla_0\cdot(\boldsymbol{T}_{t_0}^{s}(\boldsymbol{y}_0)\nabla_0 p(\boldsymbol{y}_0))||_{H^m(U)}\,\mathrm{d}s \tag{A 13}$$

holds, where γ is a constant depending on t, but not on $\nabla_0\cdot(\mathbf{T}_{t_0}^{t}(\mathbf{y}_0)\nabla_0 p(\mathbf{y}_0))$ or $\hat{\mu}$.

Proof. For a proof we refer to Igari [44]. ∎

Our assumptions on the smoothness of the nonlinearity $\mathbf{S}(\mathbf{x},\boldsymbol{\Omega}t)$, the forcing directions $\mathbf{B}(\mathbf{x},t)$ and the initial condition $p_0(\mathbf{y}_0)$ ensure that the smoothness requirements of lemma A.1 are met. The upper bound (A 13) implies directly

$$\begin{aligned}||\hat{\mu}(\mathbf{y}_0,t)-p(\mathbf{y}_0)||_{H^m(U)}&=||\xi(t)||_{H^m(U)}\\&\le\int_{t_0}^{t}\mathrm{e}^{\nu\gamma(t-s)}||\nu\nabla_0\cdot(\mathbf{T}_{t_0}^{s}(\mathbf{y}_0)\nabla_0 p(\mathbf{y}_0))||_{H^2(U)}ds\\&\le\nu\sup_{t_0\le s\le t}||\nabla_0\cdot(\mathbf{T}_{t_0}^{s}(\mathbf{y}_0)\nabla_0 p(\mathbf{y}_0))||_{H^m(U)}\frac{\mathrm{e}^{\nu\gamma(t-t_0)}-1}{\nu}\\&=\mathcal{O}(\nu).\end{aligned}$$

Since now

$$||\nabla_0\hat{\mu}(\mathbf{y}_0,t)-\nabla_0 p(\mathbf{y}_0)||_{L^\infty(U)} \le C_1||\nabla_0\hat{\mu}(\mathbf{y}_0,t)-\nabla_0 p(\mathbf{y}_0)||_{H^1(U)}$$
$$\le C_2||\hat{\mu}(\mathbf{y}_0,t)-p(\mathbf{y}_0)||_{H^2(U)}$$

holds for some constants C_1 and C_2 dependent on the dimensions of the phase space $\mathbb{R}^{2N}$, equation (A 11) holds. Therefore, leading-order transport through the surface $\mathcal{M}(t)$ can be written as stated in equation (3.6).

(b) Proof of lemma 4.3

To prove 4.3, we introduce the unit vector

$$\mathbf{e}_p(\mathbf{y}_0) := \frac{1}{|\nabla_0 p_0(\mathbf{y}_0)|}\nabla_0 p_0(\mathbf{y}_0), \tag{A 14}$$

and note that

$$\frac{|\mathbf{n}^\top(\mathbf{y}_0)\bar{\mathbf{T}}^{t_1}_{t_0}(\mathbf{y}_0)\mathbf{e}_p(\mathbf{y}_0)|}{||\bar{\mathbf{T}}^{t_1}_{t_0}(\mathbf{y}_0)||} \le \frac{|\Pi_{N_{\mathbf{y}_0}\mathcal{M}}\bar{\mathbf{T}}^{t_1}_{t_0}(\mathbf{y}_0)\mathbf{e}_p(\mathbf{y}_0)|}{||\bar{\mathbf{T}}^{t_1}_{t_0}(\mathbf{y}_0)||}, \tag{A 15}$$

since, by the Cauchy–Schwartz inequality:

$$\begin{aligned}|\mathbf{n}^\top(\mathbf{y}_0)\bar{\mathbf{T}}^{t_1}_{t_0}(\mathbf{y}_0)\mathbf{e}_p(\mathbf{y}_0)| &= |\mathbf{n}^\top(\mathbf{y}_0)[(\Pi_{N_{\mathbf{y}_0}\mathcal{M}}+\Pi_{T_{\mathbf{y}_0}\mathcal{M}})\bar{\mathbf{T}}^{t_1}_{t_0}(\mathbf{y}_0)\mathbf{e}_p(\mathbf{y}_0)]|\\ &= |\mathbf{n}^\top(\mathbf{y}_0)\Pi_{N_{\mathbf{y}_0}\mathcal{M}}\bar{\mathbf{T}}^{t_1}_{t_0}(\mathbf{y}_0)\mathbf{e}_p(\mathbf{y}_0)|\\ &\le |\Pi_{N_{\mathbf{y}_0}\mathcal{M}}\bar{\mathbf{T}}^{t_1}_{t_0}(\mathbf{y}_0)\mathbf{e}_p(\mathbf{y}_0)|,\end{aligned} \tag{A 16}$$

where we have used that $|\mathbf{n}^\top(\mathbf{y}_0|=1$. Consequently, the claim of lemma 4.3 holds, if the fraction

$$\frac{|\Pi_{N_{\mathbf{y}_0}\mathcal{M}}\bar{\mathbf{T}}^{t_1}_{t_0}(\mathbf{y}_0)\mathbf{e}_p(\mathbf{y}_0)|}{||\bar{\mathbf{T}}^{t_1}_{t_0}(\mathbf{y}_0)||}, \tag{A 17}$$

approaches zero asymptotically.

First, let us derive an upper bound on the nominator in equation (A 17):

$$\begin{aligned}|\Pi_{N_{\mathbf{y}_0}\mathcal{M}}\bar{\mathbf{T}}^{t_1}_{t_0}(\mathbf{y}_0)\mathbf{e}_p(\mathbf{y}_0)| &= \frac{1}{2|t_1-t_0|}\left|\int_{t_0}^{t_1}\Pi_{N_{\mathbf{y}_0}\mathcal{M}}[\nabla_0\mathbf{F}^t_{t_0}(\mathbf{y}_0)]^{-1}\mathbf{B}\mathbf{B}^\top[\nabla_0\mathbf{F}^t_{t_0}(\mathbf{y}_0)]^{-\top}\,dt\mathbf{e}_p(\mathbf{y}_0)\right|\\ &\le \frac{1}{2|t_1-t_0|}\int_{t_0}^{t_1}\|\Pi_{N_{\mathbf{y}_0}\mathcal{M}}[\nabla_0\mathbf{F}^t_{t_0}(\mathbf{y}_0)]^{-1}\mathbf{B}\|\,\|[\nabla_0\mathbf{F}^t_{t_0}(\mathbf{y}_0)]^{-1}\mathbf{B}\|\,\mathrm{d}t.\end{aligned} \tag{A 18}$$

Recalling that $\mathbf{B}=[\mathbf{B}_1,..,\mathbf{B}_M]$ and using the Cauchy–Schwartz inequality, we can rewrite the norm of the projection of the matrix $[\nabla_0\mathbf{F}^t_{t_0}(\mathbf{y}_0)]^{-1}\mathbf{B}$ onto the normal space $N_{\mathbf{y}_0}$ as follows:

$$\begin{aligned}\|\Pi_{N_{\mathbf{y}_0}\mathcal{M}}[\nabla_0\mathbf{F}^t_{t_0}(\mathbf{y}_0)]^{-1}\mathbf{B}\| &= \max_{\substack{\mathbf{v}\in\mathbb{R}^M\\|\mathbf{v}|=1}}|\Pi_{N_{\mathbf{y}_0}\mathcal{M}}[\nabla_0\mathbf{F}^t_{t_0}(\mathbf{y}_0)]^{-1}\mathbf{B}\mathbf{v}|\\ &= \max_{\substack{\mathbf{v}\in\mathbb{R}^M\\|\mathbf{v}|=1}}\left|\sum_{m=1}^{M}\Pi_{N_{\mathbf{y}_0}\mathcal{M}}[\nabla_0\mathbf{F}^t_{t_0}(\mathbf{y}_0)]^{-1}\mathbf{B}_m v_m\right|\\ &\le \max_{\substack{\mathbf{v}\in\mathbb{R}^M\\|\mathbf{v}|=1}}\sum_{m=1}^{M}|\Pi_{N_{\mathbf{y}_0}\mathcal{M}}[\nabla_0\mathbf{F}^t_{t_0}(\mathbf{y}_0)]^{-1}\mathbf{B}_m||v_m|\\ &\le \left(\sum_{m=1}^{M}|\Pi_{N_{\mathbf{y}_0}\mathcal{M}}[\nabla_0\mathbf{F}^t_{t_0}(\mathbf{y}_0)]^{-1}\mathbf{B}_m|^2\right)^{1/2}.\end{aligned} \tag{A 19}$$

We proceed by splitting the forcing directions $\mathbf{B}_m$ into normal and tangential direction

$$\mathbf{B}^T_m(t) := \Pi_{T_{\mathbf{y}(t)}\mathcal{M}}\mathbf{B}_m \in T_{\mathbf{y}(t)}\mathcal{M}, \quad \mathbf{B}^N_m(t) := \Pi_{N_{\mathbf{y}(t)}\mathcal{M}}\mathbf{B}_m = \mathbf{B}_m - \mathbf{B}^T_m(t) \in N_{\mathbf{y}(t)}\mathcal{M}. \tag{A 20}$$

By using the notation (A 20), we simplify the upper bound (A 19) to

$$\|\Pi_{N_{\mathbf{y}_0}\mathcal{M}}[\nabla_0\mathbf{F}^t_{t_0}(\mathbf{y}_0)]^{-1}\mathbf{B}\| \le \left(\sum_{m=1}^{M}|\Pi_{N_{\mathbf{y}_0}\mathcal{M}}[\nabla_0\mathbf{F}^t_{t_0}(\mathbf{y}_0)]^{-1}(\mathbf{B}^T_m+\mathbf{B}^N_m)|^2\right)^{1/2}$$
$$=\left(\sum_{m=1}^{M}|\Pi_{N_{\mathbf{y}_0}\mathcal{M}}[\nabla_0\mathbf{F}^t_{t_0}(\mathbf{y}_0)]^{-1}\mathbf{B}^N_m|^2\right)^{1/2}, \tag{A 21}$$

where we have used that the inverse of the linearized flow map maps the vector $\mathbf{B}^T_m(t)\in T_{\mathbf{y}(t)}\mathcal{M}$ into the tangent space $T_{\mathbf{y}_0}\mathcal{M}$ and therefore its projection into the normal space $N_{\mathbf{y}_0\mathcal{M}(t_0)}$ is zero (i.e. $\Pi_{N_{\mathbf{y}_0\mathcal{M}(t_0)}}[\nabla_0\mathbf{F}^t_{t_0}(\mathbf{y}_0)]^{-1}\mathbf{B}^T_m(t)=0$). If the forcing direction $\mathbf{B}_m$ is tangent to $\mathcal{M}$ at $\mathbf{y}(t)$, i.e. $|\mathbf{B}^N_m(t)|$ is zero, then the upper bound (A 21) is zero. For all other time instances, we have $|\mathbf{B}^N_m(t)|>0$, whereby we can rewrite equation (A 21) as follows:

$$|\Pi_{N_{\mathbf{y}_0\mathcal{M}(t_0)}}[\nabla_0\mathbf{F}^t_{t_0}(\mathbf{y}_0)]^{-1}\mathbf{B}^N_m| = |\mathbf{B}^N_m(t)|\frac{|\Pi_{N_{\mathbf{y}_0\mathcal{M}(t_0)}}[\nabla_0\mathbf{F}^t_{t_0}(\mathbf{y}_0)]^{-1}\mathbf{B}^N_m(t)|}{|\mathbf{B}^N_m(t)|}, \quad |\mathbf{B}^N_m|\neq 0. \tag{A 22}$$

We derive an upper bound for the fraction in equation (A 22) relying on the generalized Lyapunov-type numbers. Let $\mathbf{y}_0\in\mathcal{M}$ be fixed. The definition of the generalized Lyapunov-type numbers (cf. definition (4.3)) implies that for any $\delta_1>0$, there exists a time instant $t_1(\mathbf{y}_0,\delta_1)>0$ such that

$$\max_{\mathbf{w}_t\in N_{\mathbf{y}(t)\mathcal{M}}}\frac{|\mathbf{N}_{\mathbf{y}_0}(t)\mathbf{w}_t|}{|\mathbf{w}_t|} = ||\mathbf{N}_{\mathbf{y}_0}(t)|| \le (\eta(\mathbf{y}_0)+\delta_1)^{t-t_0}, \quad t>t_1(\mathbf{y}_0,\delta_1),\ \mathbf{y}_0\in\mathcal{M}. \tag{A 23}$$

Since the upper bound (A 23) holds for all vectors in the normal space $N_{\mathbf{y}(t)}\mathcal{M}$, this certainly holds for the specific choice of $\mathbf{w}_t=\mathbf{B}^N_m(t)$, which lies in the normal space $N_{\mathbf{y}(t)}\mathcal{M}$ by construction (cf. equation (A 20)). Consequently, there exists a time $t_1(\mathbf{y}_0,\delta_1)>0$ such that

$$\frac{|\Pi_{N_{\mathbf{y}_0}\mathcal{M}}\nabla_0[\mathbf{F}^t_{t_0}(\mathbf{y}_0)]^{-1}\mathbf{B}^N_m|}{|\mathbf{B}^N_m|} \le (\eta(\mathbf{y}_0)+\delta_1)^{t-t_0}, \quad t>t_1(\mathbf{y}_0,\delta_1),\ |\mathbf{B}^N_m|\neq 0, \tag{A 24}$$

which implies that

$$\left(\sum_{m=1}^{M}|\Pi_{N_{\mathbf{y}_0}\mathcal{M}(t_0)}[\nabla_0\mathbf{F}^t_{t_0}(\mathbf{y}_0)]^{-1}\mathbf{B}_m|^2\right)^{1/2} = \left(\sum_{m=1}^{M}|\mathbf{B}^N_m(t)|^2\frac{|\Pi_{N_{\mathbf{y}_0}\mathcal{M}(t_0)}[\nabla_0\mathbf{F}^t_{t_0}(\mathbf{y}_0)]^{-1}\mathbf{B}^N_m(t)|^2}{|\mathbf{B}^N_m(t)|^2}\right)^{1/2}$$
$$\le\left(\sum_{m=1}^{M}|\mathbf{B}^N_m(t)|^2\,\mathrm{e}^{2\log(\eta(\mathbf{y}_0)+\delta_1)(t-t_0)}\right)^{1/2}$$
$$\le M||\mathbf{B}||\mathrm{e}^{\log(\eta(\mathbf{y}_0)+\delta_1)(t-t_0)}$$
$$\le Mc_B\,\mathrm{e}^{\log(\eta(\mathbf{y}_0)+\delta_1)(t-t_0)}, \quad t>t_1(\mathbf{y}_0,\delta_1),\ \mathbf{y}_0\in\mathcal{M}_0, \tag{A 25}$$

where in the last step, we have used the first assumption in definition 4.1.

Moreover, the quantity $\|\Pi_{N_{\mathbf{y}_0}\mathcal{M}}[\nabla_0\mathbf{F}^t_{t_0}(\mathbf{y}_0)]^{-1}\mathbf{B}\|$ is bounded in the finite time interval $[t_0,t_1(\mathbf{y}_0,\delta_1)]$, hence can be bounded by $C_1^*\,\mathrm{e}^{\log(\eta(\mathbf{y}_0)+\delta_1)(t-t_0)}$ by selecting C_1^* appropriately. In summary, we have

$$\|\Pi_{N_{\mathbf{y}_0}\mathcal{M}}[\nabla_0\mathbf{F}^t_{t_0}(\mathbf{y}_0)]^{-1}\mathbf{B}\| \le C_1\,\mathrm{e}^{\log(\eta(\mathbf{y}_0)+\delta_1)(t-t_0)}, \quad t>t_0, \tag{A 26}$$

for some $C_1=C_1(\mathbf{y}_0,\delta_1)>0$. Furthermore, let us note that the bound (A 26) trivially holds for $\mathbf{B}^N_m=0$ (c.f. equation (A 21)).

To obtain an upper bound for the second factor in equation (A 18), we note that definition (4.4) provides an upper bound on the norm of the term $[\nabla_0 \mathbf{F}_{t_0}^t(\mathbf{y}_0)]^{-1}\mathbf{B}$:

$$\limsup_{t\to\infty} \frac{1}{t-t_0} \log(\|[\nabla_0 \mathbf{F}_{t_0}^t(\mathbf{y}_0)]^{-1}\mathbf{B}\|) \leq \limsup_{t\to\infty} \frac{1}{t-t_0} \log(c_B \|[\nabla_0 \mathbf{F}_{t_0}^t(\mathbf{y}_0)]^{-1}\|) \leq \mu_{\max}(\mathbf{y}_0), \quad \text{(A 27)}$$

where we have used the first assumption in definition 4.1 together with the monotonicity of lim sup. Thus, for any $\delta_2 > 0$, there exists some time instant $t_2(\mathbf{y}_0, \delta_2)$, such that the following holds:

$$\|[\nabla_0 \mathbf{F}_{t_0}^t(\mathbf{y}_0)]^{-1}\mathbf{B}\| \leq \mathrm{e}^{(\mu_{\max}(\mathbf{y}_0)+\delta_2)(t-t_0)}, \quad t > t_2(\mathbf{y}_0, \delta_2). \quad \text{(A 28)}$$

Since $[\nabla_0 \mathbf{F}_{t_0}^t(\mathbf{y}_0)]^{-1}\mathbf{B}$ is bounded on the finite time interval $[t_0, t_2]$, there exists some positive constant $C_2 = C_2(\delta_2, \mathbf{y}_0) > 0$ such that

$$\|[\nabla_0 \mathbf{F}_{t_0}^t(\mathbf{y}_0)]^{-1}\mathbf{B}\| \leq C_2\, \mathrm{e}^{(\mu_{\max}+\delta_2)(t-t_0)}, \quad t > t_0 \quad \text{(A 29)}$$

holds.

Finally, we estimate a lower bound on the norm of the transport tensor $\bar{\mathbf{T}}_{t_0}^{t_1}(\mathbf{y}_0)$. To this end, we note that the Euclidean norm is invariant with respect to an orthonormal coordinate change, i.e.

$$\begin{aligned}\|\bar{\mathbf{T}}_{t_0}^{t_1}(\mathbf{y}_0)\|^2 &= \max_{\substack{\mathbf{u}\in\mathbb{R}^{2N}\\ |\mathbf{u}|=1}} \langle \bar{\mathbf{T}}_{t_0}^{t_1}(\mathbf{y}_0)\mathbf{u}, \bar{\mathbf{T}}_{t_0}^{t_1}(\mathbf{y}_0)\mathbf{u}\rangle = \max_{\substack{\mathbf{u}\in\mathbb{R}^{2N}\\ |\mathbf{u}|=1}} \langle \bar{\mathbf{T}}_{t_0}^{t_1}(\mathbf{y}_0)\mathbf{u}, \mathbf{S}^\top\mathbf{S}\bar{\mathbf{T}}_{t_0}^{t_1}(\mathbf{y}_0)\mathbf{u}\rangle \\ &= \max_{\substack{\mathbf{u}\in\mathbb{R}^{2N}\\ |\mathbf{u}|=1}} \langle \mathbf{S}\bar{\mathbf{T}}_{t_0}^{t_1}(\mathbf{y}_0)\mathbf{u}, \mathbf{S}\bar{\mathbf{T}}_{t_0}^{t_1}(\mathbf{y}_0)\mathbf{u}\rangle 0 = \|\mathbf{S}\bar{\mathbf{T}}_{t_0}^{t_1}(\mathbf{y}_0)\|^2, \end{aligned} \quad \text{(A 30)}$$

holds for any orthonormal matrix $\mathbf{S}$. Thus, we obtain

$$\|\bar{\mathbf{T}}_{t_0}^{t_1}(\mathbf{y}_0)\| = \|\mathbf{S}\bar{\mathbf{T}}_{t_0}^{t_1}(\mathbf{y}_0)\| = \frac{1}{2|t_1-t_0|} \max_{\substack{\mathbf{u}\in\mathbb{R}^{2N}\\ |\mathbf{u}|=1}} \left| \mathbf{S}\int_{t_0}^{t_1} [\nabla_0 \mathbf{F}_{t_0}^t(\mathbf{y}_0)]^{-1}\mathbf{B}\mathbf{B}^\top [\nabla_0 \mathbf{F}_{t_0}^t(\mathbf{y}_0)]^{-\top}\, \mathrm{d}t\mathbf{u} \right|, \quad \text{(A 31)}$$

for any orthonormal matrix $\mathbf{S}$. Denoting the jth row of $\mathbf{S}$ by $\mathbf{s}_j \in \mathbb{R}^{1\times 2N}$ and selecting $\mathbf{S}$ such that $\mathbf{s}_1 = (\mathbf{u}^*)^\top$ (such a matrix simply consists of a orthonormal basis of $\mathbb{R}^{2N}$ with $\mathbf{u}^*$ being one the of basis vectors), it follows from the second assumption in definition 4.1 that

$$\begin{aligned}\|\bar{\mathbf{T}}_{t_0}^{t_1}(\mathbf{y}_0)\| &= \frac{1}{2|t_1-t_0|} \max_{\substack{\mathbf{u}\in\mathbb{R}^{2N}\\ |\mathbf{u}|=1}} \left[\sum_{j=1}^{2N} \left(\mathbf{s}_j \int_{t_0}^{t_1} [\nabla_0 \mathbf{F}_{t_0}^t(\mathbf{y}_0)]^{-1}\mathbf{B}\mathbf{B}^\top [\nabla_0 \mathbf{F}_{t_0}^t(\mathbf{y}_0)]^{-\top}\mathbf{u}\, dt\right)^2\right]^{\frac{1}{2}} \\ &\geq \frac{1}{2|t_1-t_0|} \max_{\substack{\mathbf{u}\in\mathbb{R}^{2N}\\ |\mathbf{u}|=1}} \int_{t_0}^{t_1} (\mathbf{u}^*)^\top [\nabla_0 \mathbf{F}_{t_0}^t(\mathbf{y}_0)]^{-1}\mathbf{B}\mathbf{B}^\top [\nabla_0 \mathbf{F}_{t_0}^t(\mathbf{y}_0)]^{-\top}\mathbf{u}\, \mathrm{d}t \\ &\geq \frac{1}{2|t_1-t_0|} \int_{t^*}^{t_1} \|(\mathbf{u}^*)^\top [\nabla_0 \mathbf{F}_{t_0}^t(\mathbf{y}_0)]^{-1}\mathbf{B}\|^2\, \mathrm{d}t \\ &\geq \frac{C_B^2}{4|t_1-t_0|\mu_{\max}(\mathbf{y}_0)} (\mathrm{e}^{2\mu_{\max}(\mathbf{y}_0)(t_1-t_0)} - \mathrm{e}^{2\mu_{\max}(\mathbf{y}_0)(t^*-t_0)}), \end{aligned} \quad \text{(A 32)}$$

where we have used the second assumption in definition 4.1. The upper bounds (A 26) and (A 29) and the lower bound (A 32) yield the following upper bound on the fraction (A 17):

$$\begin{aligned}\frac{|\mathbf{n}^\top(\mathbf{y}_0)\bar{\mathbf{T}}_{t_0}^{t_1}(\mathbf{y}_0)\mathbf{e}_p(\mathbf{y}_0)|}{||\bar{\mathbf{T}}_{t_0}^{t_1}(\mathbf{y}_0)||} &\leq \frac{\frac{1}{2|t_1-t_0|}\int_{t_0}^{t_1} C_1C_2\,\mathrm{e}^{(\log(\eta(\mathbf{y}_0)+\delta_1)+\mu_{\max}+\delta_2)(t-t_0)}\,\mathrm{d}t}{\frac{C_B^2}{4|t_1-t_0|\mu_{max}(\mathbf{y}_0)}(\mathrm{e}^{2\mu_{\max}(\mathbf{y}_0)(t_1-t_0)}-\mathrm{e}^{2\mu_{\max}(\mathbf{y}_0)(t^*-t_0)})}\\
&\leq \frac{2\mu_{\max}(\mathbf{y}_0)C_1C_2}{C_B^2|(\log(\eta(\mathbf{y}_0)+\delta_1)+\mu_{\max}+\delta_2)|}\frac{|\mathrm{e}^{(\log(\eta(\mathbf{y}_0)+\delta_1)+\mu_{\max}+\delta_2)(t_1-t_0)}-1|}{(\mathrm{e}^{2\mu_{\max}(\mathbf{y}_0)(t_1-t_0)}-\mathrm{e}^{2\mu_{\max}(\mathbf{y}_0)(t^*-t_0)})}\\
&\leq \frac{2\mu_{\max}(\mathbf{y}_0)C_1C_2}{C_B^2|(\log(\eta(\mathbf{y}_0)+\delta_1)+\mu_{\max}+\delta_2)|}\frac{\mathrm{e}^{(\log(\eta(\mathbf{y}_0)+\delta_1)-\mu_{\max}+\delta_2)(t-t_0)}+\mathrm{e}^{-2\mu_{\max}(\mathbf{y}_0)(t_1-t_0)}}{(1-\mathrm{e}^{2\mu_{\max}(\mathbf{y}_0)(t^*-t_1)})}.\end{aligned} \tag{A 33}$$

Due to the conditions (4.8), we can choose the constants δ_1 and δ_2 such that

$$\log(\eta(\mathbf{y}_0)+\delta_1)-\mu_{\min}+\delta_2<0, \tag{A 34}$$

holds. Equation (A 34) implies that all exponents in equation (A 33) are negative and hence the exponential functions in equation (A 33) decay to zero as $t_1\to\infty$. This proves lemma 4.3.

(c) Lemma 4.3 applied to NHIMs

Fenichel's [38] results apply to compact invariant manifolds of autonomous systems. To this end, we rewrite system (2.14) as an autonomous system on extended phase space $\mathbb{P}:=\mathbb{R}^{2N}\times\mathbb{T}^K$ as follows:

$$\left.\begin{aligned}\dot{\mathbf{y}}&=\mathbf{v}(\mathbf{y},\boldsymbol{\phi})\\ \text{and}\qquad \dot{\boldsymbol{\phi}}&=\boldsymbol{\Omega},\end{aligned}\right\}. \tag{A 35}$$

Then, $\mathcal{M}\times\mathbb{T}^K$ is a normally hyperbolic invariant manifold of system (A 35) by assumption. The constant growth in the phases $\boldsymbol{\phi}$ yields a zero Lyapunov exponent in this direction. Thus, a NHIM must necessarily include the phase directions, and we obtain the extended tangent space $\tilde{T}_{\mathbf{y}_0}\mathcal{M}(t_0):=T_{\mathbf{y}_0}\mathcal{M}(t_0)\times\mathbb{T}^K$. By definition (cf. Fenichel [38]), $\log(\eta(\mathbf{y}_0,\boldsymbol{\phi}_0))$ is negative along a normally hyperbolic invariant manifold. Since $\mu_{\max}$ is negative by assumption, the first and the second condition (4.8) hold.

(d) Lemma 4.3 applied to SSMs

In the following, we apply lemma 4.3 to SSMs. As Haller & Ponsioen [6] detail, for small enough ε the fixed point at the origin perturbs into a quasi-periodic solution $\mathbf{y}_\varepsilon$ and a spectral subspace E of the linear system can perturb into a SSM $W(E)$.

We consider the SSM $W(E)$ in a neighbourhood of the origin, which is a stable fixed point since the eigenvalues of the linearization have a negative real part (c.f. equation (2.17)). Thus, the SSM is locally an inflowing invarian manifold and the trajectories $\mathbf{F}_{t_0}^t(\mathbf{y}_0)$ approach the origin and thus for large enough times the forcing directions $\mathbf{B}(\mathbf{F}_{t_0}^t(\mathbf{y}),t)$ are close to the forcing evaluated at the fixed point (i.e. $\mathbf{B}(\mathbf{0},t)$). Since the forcing $\mathbf{B}(\mathbf{0},t)$ is non-degenerate by assumption, we can infer that there exists some time instance such that $\mathbf{B}(\mathbf{F}_{t_0}^t(\mathbf{y}),t)$ is non-degenerate.

Since the Lyapunov-type numbers $\eta(\mathbf{y}_0)$ and $\mu_{\max}(\mathbf{y}_0)$ are constants along trajectories, it is sufficient to calculate them at the forward time limit set of trajectories inside the SSM $W(E)$, i.e. the origin. At the origin, the linearized flow map, which can be explicitly computed:

$$\boldsymbol{\nabla}_0\mathbf{F}_{t_0}^{t_1}(\mathbf{0})=\mathrm{e}^{\mathbf{A}(t_1-t_0)}. \tag{A 36}$$

The maximal growth of the inverse of the linearized flow map $[\boldsymbol{\nabla}_0\mathbf{F}_{t_0}^{t_1}(\mathbf{0})]^{-1}$ is given by the maximal decay of $\boldsymbol{\nabla}_0\mathbf{F}_{t_0}^{t_1}(\mathbf{0})$. Thus, for the generalized Lyapunov-type exponent $\mu_{\max}(\mathbf{y}_0)$, we

obtain

$$\mu_{\max}(\mathbf{y}_\varepsilon) = -\mathrm{Re}(\lambda_{2N}), \tag{A 37}$$

where we have used equation (2.17). Since the real parts are negative by assumption, the second condition of equation (4.8) is satisfied.

To compute the generalized Lyapunov-type number $\eta(\mathbf{0})$, we collect the eigenvectors $\mathbf{v}_j$ of the linearization $\mathbf{A}$ in the matrix $\mathbf{V}$. Then, the Jordan normal form of $\mathbf{A}$ by

$$\mathbf{V} := [\mathbf{v}_1, \ldots, \mathbf{v}_{2N}], \quad \boldsymbol{\Lambda}(\tilde{\mathbf{y}}^*) = \mathbf{V}^{-1}\mathbf{A}\mathbf{V}. \tag{A 38}$$

With the Jordan normal form (A 38), we compute the inverse of the linearized flow map explicitly

$$[\nabla_0 \mathbf{F}_{t_0}^{t_1}(\tilde{\mathbf{y}}^*)]^{-1} = [\mathbf{V}^{-1}\, \mathrm{e}^{\boldsymbol{\Lambda}(t_1-t_0)}\mathbf{V}]^{-1} = \mathbf{V}^{-1}\mathrm{e}^{\boldsymbol{\Lambda}(t_0-t_1)}\mathbf{V}, \tag{A 39}$$

whereby obtain for the norm of the mapping $\mathbf{N}(t)$

$$\sup_{\substack{\mathbf{w}\in N_0E \\ |\mathbf{w}|=1}} |\Pi_{N_0E}\mathbf{V}^{-1}\, \mathrm{e}^{\boldsymbol{\Lambda}(t_0-t)}\mathbf{V}\mathbf{w}| \leq \sup_{\substack{\mathbf{w}\in N_0E \\ |\mathbf{w}|=1}} |\mathrm{e}^{\boldsymbol{\Lambda}(t_0-t)}\mathbf{V}\mathbf{w}|. \tag{A 40}$$

Since the vector $\mathbf{w}$ is in normal space N_0E, i.e. orthogonal to E, it excites only the directions not included in E. Thus, the generalized Lyapunov-type number is determined by the spectrum not included in E., i.e.

$$\begin{aligned} &\sup_{\substack{\mathbf{w}\in N_0E \\ |\mathbf{w}|=1}} |\Pi_{N_0E}\mathbf{V}^{-1}\, \mathrm{e}^{\boldsymbol{\Lambda}(t_0-t)}\mathbf{V}\mathbf{w}| \\ &\leq \max_{\lambda\in \mathrm{spect}(\mathbf{A})-\mathrm{spect}(\mathbf{A}|_E)} \mathrm{e}^{-\mathrm{Re}(\lambda)(t-t_0)} = \mathrm{e}^{-\min_{\lambda\in\mathrm{spect}(\mathbf{A})-\mathrm{spect}(\mathbf{A}|_E)}(\mathrm{Re}(\lambda))(t-t_0)}. \end{aligned} \tag{A 41}$$

Together with equation (A 37), we obtain for the first condition in equation (4.8) of lemma 4.3

$$\log(\eta(\mathbf{y}_0)) \leq -\min_{\lambda\in\mathrm{spect}(\mathbf{A})-\mathrm{spect}(\mathbf{A}|_E)} \mathrm{Re}(\lambda) < -\mathrm{Re}(\lambda_{2N}) = \mu_{\min}(\mathbf{y}_0), \quad \text{for all } \mathbf{y}_0 \in W(E), \tag{A 42}$$

which is satisfied, if condition (4.9) holds. This proves the claim of theorem 4.9.

References

1. Guckenheimer J, Holmes P. 2002 *Nonlinear oscillations, dynamical systems, and bifurcations of vector fields*, vol. 42, Ed. 2002. Applied mathematical sciences, corr. 7th printing edn. New York: Springer.
2. Wiggins S. 2013 *Normally hyperbolic invariant manifolds in dynamical systems*, vol. 105. New York, NY: Springer Science & Business Media.
3. Lutes LD, Sarkani S. 2004 *Random vibrations: analysis of structural and mechanical systems*. London, UK: Butterworth-Heinemann.
4. Kerschen G, Peeters M, Golinval J, Vakakis A. 2009 Nonlinear normal modes, part I: a useful framework for the structural dynamicist. *Mech. Syst. Signal Process.* **23**, 170–194. (doi:10.1016/j.ymssp.2008.04.002)
5. Shaw S, Pierre C. 1993 Normal modes for non-linear vibratory systems. *J. Sound Vib.* **164**, 85–124. (doi:10.1006/jsvi.1993.1198)
6. Haller G, Ponsioen S. 2016 Nonlinear normal modes and spectral submanifolds: existence, uniqueness and use in model reduction. *Nonlinear Dyn.* **86**, 1493–1534. (doi:10.1007/s11071-016-2974-z)
7. Jain S, Tiso P, Haller G. 2018 Exact nonlinear model reduction for a von kármán beam: Slow-fast decomposition and spectral submanifolds. *J. Sound Vib.* **423**, 195–211. (doi:10.1016/j.jsv.2018.01.049)
8. Breunung T, Haller G. 2018 Explicit backbone curves from spectral submanifolds of forced-damped nonlinear mechanical systems. *Proc. R. Soc. A* **474**, 20180083. (doi:10.1098/rspa.2018.0083)

9. Ponsioen S, Jain S, Haller G. 2020 Model reduction to spectral submanifolds and forced-response calculation in high-dimensional mechanical systems. *J. Sound Vib.* **488**, 115640. (doi:10.1016/j.jsv.2020.115640)
10. Jain S, Haller G. 2022 How to compute invariant manifolds and their reduced dynamics in high-dimensional finite element models. *Nonlinear Dyn.* **107**, 1417–1450.
11. Rubinstein RY, Kroese DP. 2016 *Simulation and the Monte Carlo method*, vol. 10. Hoboken, NJ: John Wiley & Sons.
12. Berglund N, Gentz B. 2003 Geometric singular perturbation theory for stochastic differential equations. *J. Differ. Equ.* **191**, 1–54. (doi:10.1016/S0022-0396(03)00020-2)
13. Schmalfuss B, Schneider KR. 2008 Invariant manifolds for random dynamical systems with slow and fast variables. *J. Dyn. Differ. Equ.* **20**, 133–164. (doi:10.1007/s10884-007-9089-7)
14. Kuehn C. 2015 *Multiple time scale dynamics*, **vol. 191**. Springer.
15. Kerschen G, Worden K, Vakakis AF, Golinval J-C. 2006 Past, present and future of nonlinear system identification in structural dynamics. *Mech. Syst. Signal Process.* **20**, 505–592. (doi:10.1016/j.ymssp.2005.04.008)
16. Li J, Lu K, Bates P. 2013 Normally hyperbolic invariant manifolds for random dynamical systems: part I-persistence. *Trans. Am. Math. Soc.* **365**, 5933–5966. (doi:10.1090/S0002-9947-2013-05825-4)
17. Wanner T. 1995 Linearization of random dynamical systems. In *Dynamics reported*, pp. 203–268. Springer.
18. Arnold L. 2003 *Random dynamical systems*. Springer monographs in mathematics, [corr. 2nd print.] edn. Berlin, Germany: Springer.
19. Mohammed S-EA, Scheutzow MK. 1999 The stable manifold theorem for stochastic differential equations. *Ann. Probab.* **27**, 615–652. (doi:10.1214/aop/1022677380)
20. Risken H. 1996 Fokker-planck equation. In *The Fokker-Planck Equation*, pp. 63–95. Springer.
21. Caughey T, Ma F. 1982 The steady-state response of a class of dynamical systems to stochastic excitation. *J. Appl. Mech.* **49**, 629–632. (doi:10.1115/1.3162538)
22. Lin Y, Cai G. 2004 *Probabilistic structural dynamics: advanced theory and applications*. McGraw-Hill engineering reference. New York: McGraw-Hill.
23. Soize C. 1994 *The Fokker-Planck equation for stochastic dynamical systems and its explicit steady state solutions*, vol. 17. Singapore: World Scientific.
24. Atkinson J. 1973 Eigenfunction expansions for randomly excited non-linear systems. *J. Sound Vib.* **30**, 153–172. (doi:10.1016/S0022-460X(73)80110-5)
25. Ibrahim RA. 1995 Recent results in random vibrations of nonlinear mechanical systems. *J. Vib. Acoust.* **117**, 222–233. (doi:10.1115/1.2838667)
26. Crandall SH. 1980 Non-gaussian closure for random vibration of non-linear oscillators. *Int. J. Non-Linear Mech.* **15**, 303–313. (doi:10.1016/0020-7462(80)90015-3)
27. Stratonovich R, Silverman RA. 1963 *Topics in the theory of random noise*, vol. 3. Mathematics and its applications, [etc., rev. english ed. edition]. New York: Gordon and Breach.
28. Roberts J, Spanos P. 1986 Stochastic averaging: an approximate method of solving random vibration problems. *Int. J. Non-Linear Mech.* **21**, 111–134. (doi:10.1016/0020-7462(86)90025-9)
29. Roberts J, Spanos P. 1990 *Random vibration and statistical linearization*. Chichester, UK: Wiley.
30. Haller G, Karrasch D, Kogelbauer F. 2020 Barriers to the transport of diffusive scalars in compressible flows. *SIAM J. Appl. Dyn. Syst.* **19**, 85–123. (doi:10.1137/19M1238666)
31. Vig JR, Kim Y. 1999 Noise in microelectromechanical system resonators. *IEEE Trans. Ultrason. Ferroelectr. Freq. Control* **46**, 1558–1565. (doi:10.1109/58.808881)
32. Shoshani O, Heywood D, Yang Y, Kenny TW, Shaw SW. 2016 Phase noise reduction in an mems oscillator using a nonlinearly enhanced synchronization domain. *J. Microelectromech. Syst.* **25**, 870–876. (doi:10.1109/JMEMS.2016.2590881)
33. Williams D, Chris L, Rogers G., 1987 *Itô calculus*, vol. 2. Diffusions, Markov processes, and martingales. Chichester: Wiley.
34. Øksendal BK. 2010 *Stochastic differential equations: an introduction with applications*. Universitext. Berlin, Germany: Springer.
35. Szalai R, Ehrhardt D, Haller G. 2017 Nonlinear model identification and spectral submanifolds for multi-degree-of-freedom mechanical vibrations. *Proc. R. Soc. A* **473**, 20160759.
36. Cabré X, Fontich E, de la Llave R. 2003 The parameterization method for invariant manifolds I: manifolds associated to non-resonant subspaces. *Ind. Univ. Math. J.* **52**, 283–328. (doi:10.1512/iumj.2003.52.2245)

37. Haro A, de la Llave R. 2006 A parameterization method for the computation of invariant tori and their whiskers in quasi-periodic maps: rigorous results. *J. Differ. Equ.* **228**, 530–579. (doi:10.1016/j.jde.2005.10.005)
38. Fenichel N. 1972 Persistence and smoothness of invariant manifolds for flows. *Indiana Univ. Math. J.* **21**, 193–226. (doi:10.1512/iumj.1972.21.21017)
39. Chicone C. 2006 *Ordinary differential equations with applications*. New York: Springer.
40. Oseledec VI. 1968 A multiplicative ergodic theorem. Characteristic ljapunov, exponents of dynamical systems. *Trudy Moskovskogo Matematicheskogo Obshchestva* **19**, 179–210.
41. Ott W, Yorke JA. 2008 When lyapunov exponents fail to exist. *Phys. Rev. E* **78**, 056203. (doi:10.1103/PhysRevE.78.056203)
42. Tang X, Boozer A. 1996 Finite time lyapunov exponent and advection-diffusion equation. *Physica D* **95**, 283–305. (doi:10.1016/0167-2789(96)00064-4)
43. Thiffeault J-L. 2003 Advection-diffusion in lagrangian coordinates. *Phys. Lett. A* **309**, 415–422. (doi:10.1016/S0375-9601(03)00244-5)
44. Igari K. 1974 Degenerate parabolic differential equations. *Publ. Res. Inst. Math. Sci.* **9**, 493–504. (doi:10.2977/prims/1195192569)